Invasion of white matter tracts by glioma stem cells is regulated by a *NOTCH1–SOX2* positive-feedback loop

Jun Wang[1,2,12], Sen-Lin Xu[1,12], Jiang-Jie Duan[1,2,12], Liang Yi[3,12], Yu-Feng Guo[1,2], Yu Shi[1], Lin Li[1,2], Ze-Yu Yang[1,2], Xue-Mei Liao[1,2], Jiao Cai[1,2], Yan-Qi Zhang[4], Hua-Liang Xiao[5], Li Yin[1,2], Hao Wu[6], Jing-Na Zhang[7], Sheng-Qing Lv[8], Qing-Kai Yang [9], Xiao-Jun Yang[10], Tao Jiang[11], Xia Zhang[1], Xiu-Wu Bian [1]* and Shi-Cang Yu [1,2]*

Early invasive growth along specific anatomical structures, especially the white matter tract, is regarded as one of the main causes of poor therapeutic outcome of people with gliomas. We show that some glioma stem cells (GSCs) are preferentially located along white matter tracts, which exhibit a demyelinated phenotype, at the invasive frontier of glioma tissues. These GSCs are CD133⁺Notch1⁺, whereas the nerve fibers express the Notch ligand Jagged1. The Notch-induced transcription factor Sox9 promotes the transcription of *SOX2* and the methylation level of the *NOTCH1* promoter is attenuated by the upregulation of *SOX2* to reinforce *NOTCH1* expression in GSCs. This positive-feedback loop in a cohort of glioma subjects is correlated with a poor prognosis. Inhibition of Notch signaling attenuates the white-matter-tract tropism of GSCs. These findings provide evidence indicating that the *NOTCH1-SOX2* positive-feedback loop controls GSC invasion along white matter tracts.

Malignant glioma is the most common type of primary malignant tumor in the central nervous system. Despite advances in surgery, radiation and chemotherapy treatments, the overall 5-year survival rate for people with this type of tumor remains <10% (ref. [1–4]). Early invasive growth along white matter tracts, perivascular space and meninges is the most prominent clinicopathological characteristic of malignant glioma and is regarded as one of the main causes of a poor therapeutic outcome[1–4]. It is important to understand whether glioma cells randomly reach these existing structures or whether these anatomical components attract glioma cells and then provide advantages for the survival of these cells[4]. Unfortunately, knowledge regarding this is limited[4].

Recently, it has been shown that different types of tumor progenitor cells and cancer stem cells (CSCs), including glioma stem cells (GSCs), preferentially reside in perivascular regions. Nestin⁺CD133⁺ GSCs are located next to capillaries in malignant glioma[5]. Abundant nutrition diffuses from blood vessels, and certain soluble factors that are secreted by vascular endothelial cells attract GSCs, causing GSCs to migrate to perivascular regions. This vascular niche is endowed with the ability to sustain GSCs's stemness[5,6]. Increasing the quantity of blood vessels in orthotopic xenografts increases the number of self-renewing GSCs and accelerates tumor initiation and growth[5]. More important, according to

the fundamental role of GSCs in glioma development[4,7], this spatial distribution of GSCs might be the main reason for the early invasion of glioma along the perivascular space.

However, the spatial relationship between GSCs and white matter tracts, other anatomical structures along which glioma cells preferentially migrate, remains unknown. Whether this distribution of glioma is mediated by the attraction of soluble factors or by specific ligand-receptor interaction between GSCs and white matter tracts is unclear. Exploring the mechanisms behind this will help us not only to understand the biology of white-matter-tract tropism, which is thought to explain the noncurative surgical resection of gliomas, but also to discover promising brain-specific therapeutic targets for this damaging tumor.

In this study, we show that white matter tracts activated the *NOTCH1-SOX9-SOX2* positive-feedback loop in GSCs via Jagged1. This interaction may provide certain survival advantages for GSCs. Thus, we propose that the white matter tracts form niche microenvironments that promote expression of the core stemness transcription factor for GSCs and represent therapeutic targets in brain tumors.

Results

CD133⁺ GSCs preferentially locate along white matter tracts. To establish whether GSCs exhibit white-matter-tracts tropism, we first

[1]Institute of Pathology and Southwest Cancer Center, Key Laboratory of the Ministry of Education, Southwest Hospital, Army Medical University (Third Military Medical University), Chongqing, China. [2]Department of Stem Cell and Regenerative Medicine, Southwest Hospital, Army Medical University (Third Military Medical University), Chongqing, China. [3]Department of Neurosurgery, Daping Hospital, Army Medical University (Third Military Medical University), Chongqing, China. [4]Department of Medical Statistics, Military Preventive Medicine Academy, Army Medical University (Third Military Medical University), Chongqing, China. [5]Department of Pathology, Daping Hospital, Army Medical University (Third Military Medical University), Chongqing, China. [6]Department of Radiology, Daping Hospital, Army Medical University (Third Military Medical University), Chongqing, China. [7]Department of Medical Imaging, College of Biomedical Engineering, Army Medical University (Third Military Medical University), Chongqing, China. [8]Department of Neurosurgery, Xinqiao Hospital, Army Medical University (Third Military Medical University), Chongqing, China. [9]Institute of Cancer Stem Cell, Cancer Center, Second Affiliated Hospital, Dalian Medical University, Dalian, China. [10]Center for Neuroscience, Medical College, Shantou University, Shantou, China. [11]Department of Neurosurgery, TianTan Hospital, Capital Medical University, Beijing, China. [12]These authors contributed equally: Jun Wang, Sen-Lin Xu, Jiang-Jie Duan, Liang Yi. *e-mail: bianxiuwu@263.net; yushicang@163.com

determined the incidence of CD133^{+} cells and the proximity of these cells to nerve fibers in brain-tumor tissue interfaces (Fig. 1a,b).

In contrast to the low incidence of GSCs within the total glioma tissue[8], about 5.01–15.13% of glioma cells within this region were CD133^{+}. These CD133^{+} glioma cells were mixed together with the tangling nerve fibers (Supplementary Fig. 1a and Fig. 1c) and located close to nerve fibers (Fig. 1d,e). The distance between 26 CD133^{+} cells (3.25%) and the nerve fibers was within 1 μm. Only 50.5% (404/800) of CD133^{+} cells were located at least 5 μm away from the nerve fibers (Fig. 1f). Other markers, including CDC6, PBK[9] and CD44 (ref. [10]), were also used to label the GSC subpopulation. In addition to CD44^{+} cells, CDC6^{+} and PBK^{+} cells were also adjacent to nerve fibers (Supplementary Fig. 1b,c). Notably, the white matter tracts around the tumor swelled significantly, and the myelin seemed discontinuous (Fig. 1g). The signals for Tau1 or NF200 and myelin basic protein (MBP) did not overlap, and some white matter tracts were presented in a MBP-intermittent or MBP-negative manner (Fig. 1h,i). These results suggest that some GSCs in the glioma-brain interface are preferentially located adjacent to unmyelinated white matter tracts.

Jagged1 and Notch1 interaction determines GSCs' distribution. To determine whether the white-matter-tract tropism of GSCs requires direct cell-cell contact or whether it is mediated by soluble factors secreted by neurons, a transwell assay was used with the culture supernatant of neurons as a chemoattractant. However, there were no significant differences in GSC number between the neuron-supernatant group and the control group (Supplementary Fig. 2a,b). Although this result does not exclude the potential role performed by soluble factors in regulating the white-matter-tract tropism of GSCs, we still wanted to assess whether the direct interaction of receptors and ligands had a role in this process.

As has been mentioned in a previous study, endothelial cells can promote the colorectal CSC phenotype through activated Notch signaling[11]. Notably, during central nervous system development, axonally expressed Jagged1, a Notch ligand, has a critical role in controlling neuron differentiation and myelination[12,13]. Therefore, we explored the interaction of Notch ligands and receptors in determining the white-matter-tract tropism of GSCs. In human glioma samples, these nerve fibers at the invasive frontier all expressed Jagged1, the distribution of which was diffuse (Fig. 2a,b). A total of 26 Jagged1^{+} signals (3.2%) were located within 1 μm of nerve fibers. Only 45.1% (363/805) of the Jagged1^{+} signals were at least 5 μm away from the nerve fibers (Fig. 2c). Coexpression of Jagged1 and Tau1 was also detected in the axons of neurons cultured in vitro (Fig. 2d). Moreover, nearly all CD133^{+} GSCs were also Notch1^{+} (Fig. 2e,f). This positive correlation was manifested in the Pollard data set (Fig. 2g). In addition, the positive correlation between the expression of NOTCH1 and the stemness score[14] was also observed in the TCGA-540 data set (Fig. 2h). Fluorescent staining further demonstrated that scattered Notch1^{+} GSCs were distributed along nerve fibers (Fig. 2i,j).

We then cocultured glioma cells with human neurons. CD133^{+} GSCs presented more axon tropism than CD133^{−} non-GSCs (Supplementary Fig. 2c). After NOTCH1 expression was knocked down or the binding between Notch1 and Jagged1 was inhibited by Decoy, few GSCs made contact with the axons (Supplementary Fig. 3d,e). The NOTCH1-downregulated GL261-GSCs were then implanted into the right striatum adjacent to the corpus callosum in Thy1-EGFP mice (Fig. 3a). At 2 weeks after implantation, some glioma cells invaded along the white matter tracts in the control group, although the tumor mass at the site of inoculation was not obvious (Fig. 3b). Conversely, rare glioma cells were detected in the NOTCH1-knockdown group (Fig. 3b,c). More important, most of the glioma cells distributed along or inside the white matter tracts were CD133^{+} and CD44^{−} (Fig. 3d,e; Supplementary Fig. 2f).

At 4 weeks after implantation, multiple tumor lesions on the opposite side of the brain midline, ipsilateral hippocampus and contralateral hippocampus were observed in the control group (Fig. 3f), demonstrating the invasive growth of GSCs along the corpus callosum or other projection fibers (Supplementary Fig. 2g). However, the tumors grew only near the site of implantation in the NOTCH1-knockdown group (Fig. 3f). These results indicate that activation of the Notch signaling pathway in GSCs controls the white-matter-tract tropism of GSCs.

NOTCH1 upregulates the transcription of SOX2 via SOX9. Next, we aimed to understand the survival advantages provided to GSCs by activation of the Notch signaling pathway. SOX2 (sex-determining region Y-box 2) encodes the core transcription factor for maintaining stemness[15]. Sox2^{+} glioma cells were mixed together with tangled nerve fibers (Fig. 4a) and located close to nerve fibers, similar to CD133^{+} or Notch1^{+} cells (Fig. 4a,b). The positive correlation between SOX2 expression and the stemness score[14] was manifested in the TCGA-540 cohort (Fig. 4c). In addition, we further cocultured CD133^{+} GSCs with human neurons. After SOX2 expression was knocked down, the number of GSCs decreased and the cells made contact with the axons (Fig. 4d). Moreover, NOTCH1 expression was positively correlated with SOX2 expression in three published data sets (Supplementary Fig. 3a). The association between SOX2 and the other three Notch receptor–coding genes (NOTCH2–NOTCH4) was relatively weaker than that between SOX2 and NOTCH1 (Supplementary Fig. 3b–d). In addition, the association between the mRNA expression of NOTCH1 and SOX2 was assessed using microarray data sets containing the expression data for GSCs, neural stem cells (NSCs), differentiated glioma cells (non-GSCs) and normal cortex tissue. This positive relationship was observed only in GSCs, indicating that it was specific to the GSC subpopulation (Fig. 4e,f). In two primary glioblastoma cultures (GBM1 and GBM2) and the U87 cell line, we knocked down NOTCH1 in the GSCs and overexpressed it in the non-GSC subpopulation. The mRNA and protein levels of SOX2 increased and decreased, respectively, as did the expression of NOTCH1 and activation of the Notch signaling pathway (Fig. 4g–j).

We then investigated whether SOX2 was transcriptionally regulated by NOTCH1 in human GSCs. Luciferase reporters containing the 5′-promoter regions (−2237 to +111 bp) of SOX2 were expressed in NOTCH1-overexpressing GBM2 cells, and luciferase activities were notably altered (Supplementary Fig. 4a). The recombinant binding protein suppressor of hairless-κ (RBP-Jκ), the core transcription factor of the Notch signaling pathway, can directly bind the promoter of sox2 and initiate the transcription of sox2 in mouse NSCs[16]. However, there are significant differences between the human SOX2 and mouse sox2 promoter regions (Supplementary Fig. 4b). After using a chromatin immunoprecipitation (ChIP) assay, we performed PCR to amplify the two putative binding sites of RBP-Jκ in the human SOX2 promoter. RBP-Jκ did not bind to these sites (Supplementary Fig. 4c,d). Because Notch activation initiates the expression of downstream Notch-induced transcription factors (NTFs), including HEY-1, HEY-2, HES-1 and SOX9 (sex-determining region Y-box 9), and then promotes the transcription of target genes[17], the association between the expression of SOX2 and these NTFs was assessed with the three data sets mentioned above. SOX2 expression was positively correlated with the expression of SOX9 (Supplementary Fig. 3e). The association between SOX2 and the other three NTFs was relatively weaker than that between SOX2 and SOX9 (Supplementary Fig. 3f–h). In human glioma samples, Sox9^{+} glioma cells mixed with the tangled nerve fibers Fig. 4k) were located close to nerve fibers, similarly to CD133^{+}, Notch1^{+} or Sox2^{+} cells (Fig. 4k,l). SOX9 expression and the stemness score[14] were positively correlated in the TCGA-540 cohort (Fig. 4m), and so were SOX2 and NOTCH1 expression (Fig. 4n). Meanwhile, the coexpression
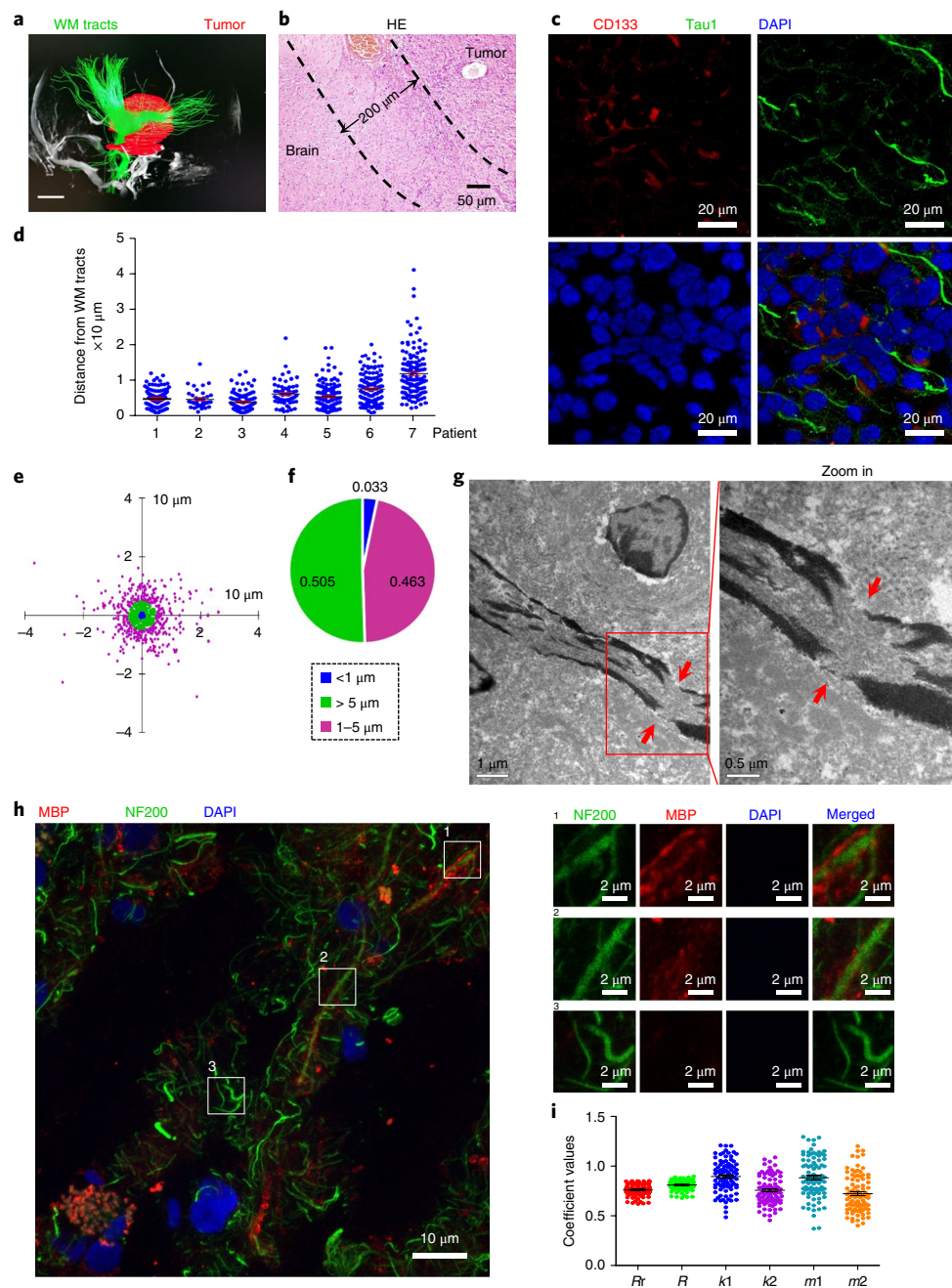
Fig. 1 | White-matter-tract tropism of glioma stem cells. a, A 3D model reconstruction of a glioma subject by diffusion tensor imaging for noninvasive fiber tracing (nerve fiber tracts, green; tumor tissue, red). Representative image derived from seven glioma subjects. WM, white matter. **b**, Hematoxylin-eosin (HE) staining of 0.5 mm³ glioma tissue derived from a 200-μm region beyond the macroscopic boundary. Representative image derived from seven subjects (3 sections per subject). The invasive frontier is the region between the two dashed lines. Scale bar, 50 μm. **c–f**, Spatial relationship between GSCs (CD133⁺, red) and nerve fibers (Tau1⁺, green) at the invasive frontier of glioma subjects. Seven subjects, three female and four male, aged 20–63, three sections per subject, 173 fields and 800 CD133⁺ cells in total ($n_1 = 152$; $n_2 = 38$; $n_3 = 121$; $n_4 = 62$; $n_5 = 143$; $n_6 = 149$; $n_7 = 135$). Representative images of nuclei stained with DAPI (blue) are shown. Scale bar, 20 μm (**c**). Quantitative analysis of the minimum distance of every GSC from nerve fibers in seven glioma subjects (subject 1, 0.450 ± 0.229 μm; subject 2, 0.437 ± 0.262 μm ; subject 3, 0.358 ± 0.239 μm; subject 4, 0.587 ± 0.347 μm; subject 5, 0.512 ± 0.346 μm; subject 6, 0.725 ± 0.394 μm ; subject 7, 1.157 ± 0.668 μm) (**d**). Quantitative analysis of spatial orientation of every GSC ($n = 800$) to the nearest nerve fibers (**e**). Quantitative analysis of proportion of GSCs at the following distances from the nerve fibers: <1 μm; 1–5 μm; and >5 μm (**f**). **g**, Left: representative image of white matter tracts adjacent to tumor tissue; scale bar, 1 μm. Right: expanded view of inset region (red box) in left panel; scale bar, 0.5 μm (female, aged 40). Seven subjects, three female and four male, aged 42–63, three sections per subject. Swelled white matter tract and discontinuous myelin are indicated by red arrowhead. Scale bar, 500 nm. **h**, NF200/Tau-1 and MBP double-immunofluorescence staining of white matter tracts at invasive frontier of glioma subjects. Three samples, three sections per sample, ten fields per section. Left: representative images of different regions of nerve fibers. Nuclei stained with DAPI (blue) are shown; scale bar, 10 μm. Right: expanded view of inset regions (white box) in left panel; scale bar, 2.0 μm. **i**, Correlation and overlap coefficients of MBP/Tau1 expression. Three subjects, male, aged 29–63, three sections per subject, ten fields per section, 90 fields in total. Rr, Pearson's correlation coefficient (0.761 ± 0.058); R, Mander's overlap coefficient (0.811 ± 0.050); k, overlap coefficients ($k1$, red fluorescent signal, 0.895 ± 0.161; $k2$, green fluorescent signal, 0.757 ± 0.140); m, colocalization coefficients ($m1$, red fluorescent signal, 0.884 ± 0.205; $m2$, green fluorescent signal, 0.723 ± 0.188).
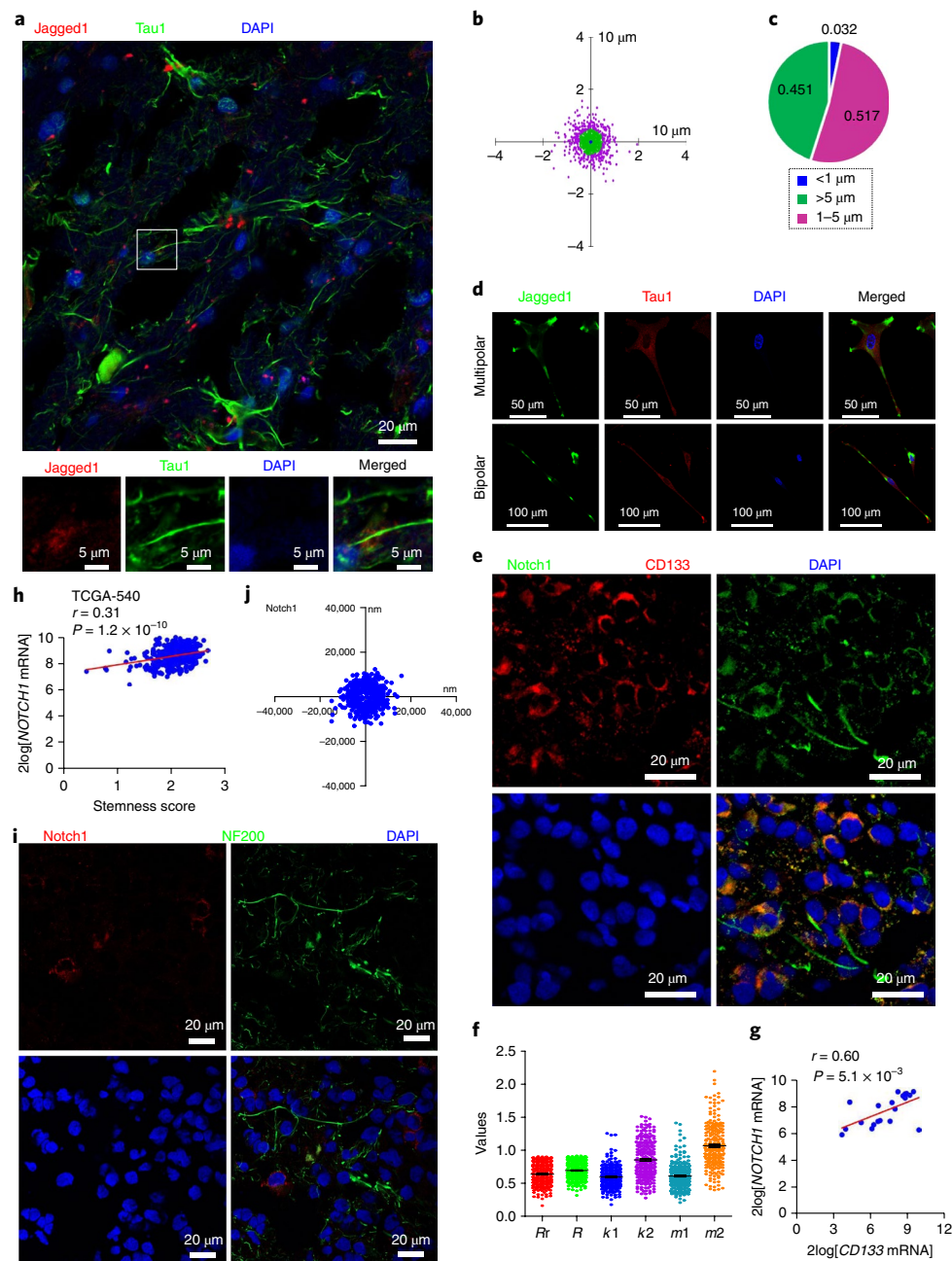
Fig. 2 | CD133$^+$Notch1$^+$ GSCs distributed along with Jagged1$^+$ nerve fibers (Tau1$^+$). a–c, Spatial relationship between Jagged1$^+$ (red) and nerve fibers (Tau1$^+$, green) at the invasive frontier of glioma subject as detected by immunofluorescence staining. Top: representative laser confocal microscopy images of nuclei stained with DAPI (blue) are shown. Seven subjects, two female and five male, aged 20–72 years, three sections per sample, 161 fields in total, scale bar, 20 μm. Bottom: expanded view of inset region (white box) in top panel; scale bar, 5.0 μm (**a**). Quantitative analysis of spatial orientation of every Jagged1 signal ($n = 805$) to the nearest nerve fiber (**b**). Quantitative analysis of proportion of Jagged1 signals at the following distances from nerve fibers: <1 μm; 1–5 μm; and >5 μm (**c**). **d**, Expression of Jagged1 (green) and Tau (red) in neurons cultured in vitro, as detected by immunofluorescence staining. Representative laser confocal microscopy images derived from 26 neurons cultured in vitro. Nuclei stained with DAPI (blue) are shown. Scale bars, 50 μm (top), 100 μm (bottom). **e,f**, Expression of CD133 (red) and Notch1 (green) at invasive frontier of a glioma subject detected by immunofluorescence staining. Eight samples, four female and four male, aged 20–63 years, three sections per sample, 235 fields in total. Representative laser confocal microscopy images of nuclei stained with DAPI (blue) are shown. Scale bar, 20 μm (**e**). The correlation and overlap coefficients of CD133 and Notch1 expression were calculated using Colocalizer Pro for Mac 3.0.2. Rr, Pearson's correlation coefficient (0.638 ± 0.167); R, Mander's overlap coefficient (0.692 ± 0.138); k, overlap coefficients ($k1$, red fluorescent signal, 0.593 ± 0.165; $k2$, green fluorescent signal, 0.853 ± 0.281); m, colocalization coefficients ($m1$, red fluorescent signal, 0.608 ± 0.197; $m2$, green fluorescent signal, 1.067 ± 0.330) (**f**). **g**, Correlation between *CD133* and *NOTCH1* mRNA levels in GSCs. Expression data were derived from glioblastoma stem cells (Pollard data set, Pearson correlation, $n = 20$ biologically independent samples, two-tailed). **h**, Correlation between *NOTCH1* mRNA levels and stemness score. Expression data were derived from glioblastoma (540 data set, Pearson correlation, $n = 424$ biologically independent samples, two-tailed). **i,j**, Spatial relationship between Notch1$^+$ cells (red) and nerve fibers (NF200$^+$, green) at the invasive frontier of glioma subjects, as detected by immunofluorescence staining. Three samples, three sections per sample, three males, aged 46–57 years, ten fields per section, 450 independent Notch1$^+$ cells in total. Representative laser confocal microscopy images of nuclei stained with DAPI (blue) are shown. Scale bar, 20 μm (**i**). Quantitative analysis of minimum distance of every Notch1$^+$ cell from nerve fibers in three glioma subjects (**j**).
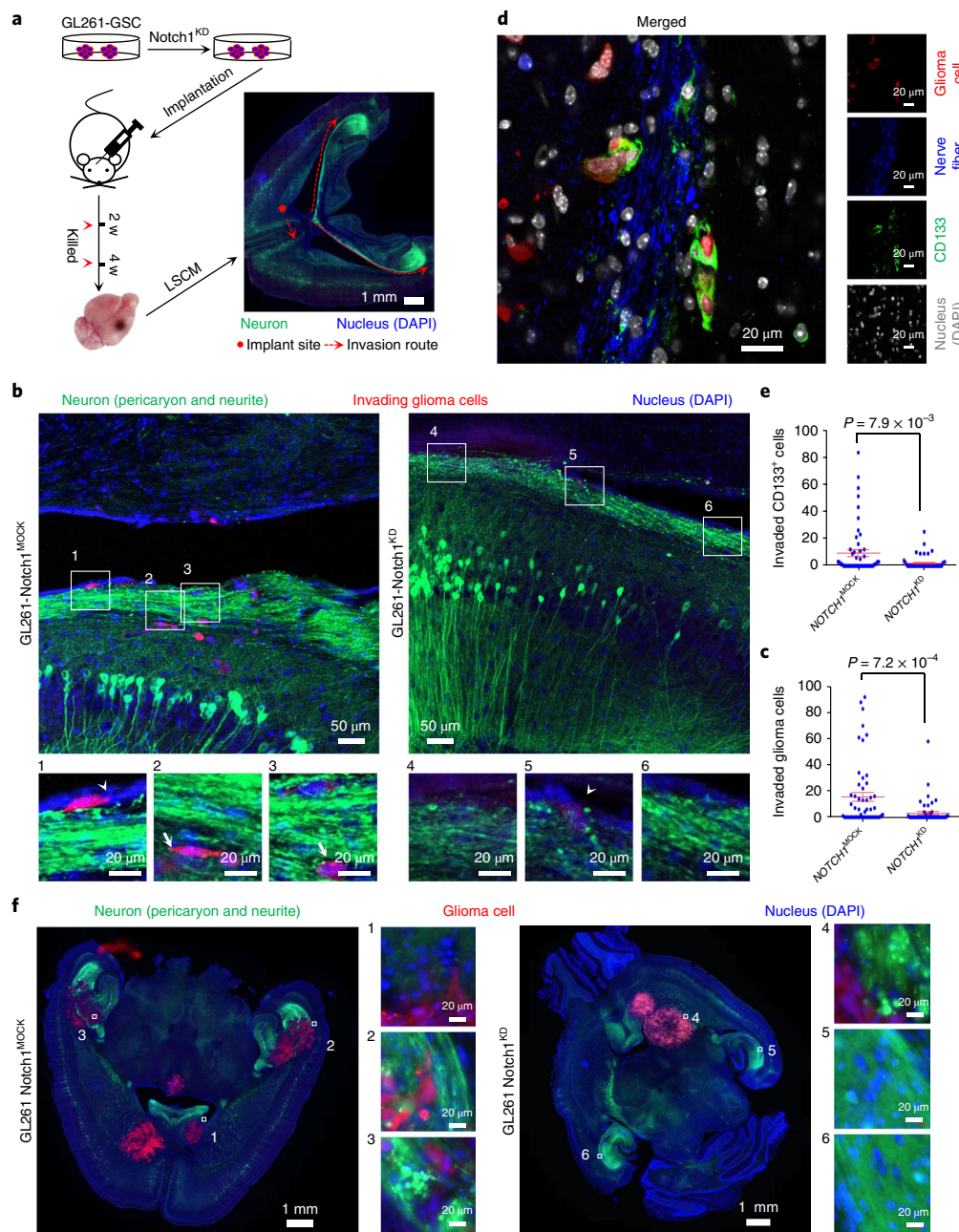
Fig. 3 | Notch signaling pathway activity in GSCs controls white-matter-tract tropism of GSCs. a, Schematic diagram of orthotopic xenografts ($n = 3$ mice, two female and one male, aged 4–5 weeks (w)). Right: whole brain tissue. Red circle, site of implantation; dotted arrow, route of invasion. Scale bar, 1 mm. **b,c**, Two weeks after orthotopic implantation of 1×10^5 mCherry-labeled GL261 GSCs into the right striatum, adjacent to the corpus callosum, in Thy1-EGFP transgenic mice. Green, neuron (including perikaryon and neurite); red, glioma cells. White arrowhead, glioma cells inside the white matter tracts; white arrow, glioma cells outside the white matter tracts. Representative full-slice scanner images of nuclei stained with DAPI (blue) are shown. **b**, Top: different regions of white matter tracts adjacent to hippocampus indicate the invading glioma cells. Scale bar, 50 μm. GL261 cells transfected with control vector (GL216-$NOTCH1^{MOCK}$, left) vs. GSCs transfected with $NOTCH1$-shRNA vector (GL261-$NOTCH1^{KD}$, right). Bottom: expanded view of inset regions (white box) in top panel. Insets 1–6, scale bar, 20 μm. **c**, Quantitative analysis of invading glioma cells along white matter tracts. Three mice per group, three sections per mouse, three to six high-power fields per section. Data are presented as mean ± s.d. Nonparametric tests (Mann–Whitney, $n = 54$ independent high-power fields, two-tailed) were used to generate P values, mock vs. $NOTCH1^{KD}$. **d,e**, Immunofluorescence staining of CD133 (green) in xenografts of the control group to reveal invasive growth of glioma cells (red) along the nerve fibers (blue). Five mice per group, three sections per mouse, three to six high-power fields per section. Representative laser confocal microscopy images of nuclei stained with DAPI (gray) are shown. Scale bar, 20 μm. (**d**). Quantitative analysis of invading CD133+ glioma cells along white matter tracts. Data are presented as mean ± s.d. Nonparametric test (Mann–Whitney, $n = 54$ independent high-power fields, two-tailed) was used to generate P values, mock vs. $NOTCH1^{KD}$ (**e**). **f**, Four weeks after orthotopic implantation of mCherry-labeled GL261 GSCs into the right striatum, adjacent to the corpus callosum, of Thy1-EGFP transgenic mice. Green, neuron (including perikaryon and neurite); red, glioma cells. Three mice per group, three sections per mouse, six high-power fields per section, $n = 54$ independent high-power fields. Left: representative full-slice scanner images of nuclei stained with DAPI (blue). Scale bar, 1 mm. GL261 cells transfected with control vector (GL261-$NOTCH1^{MOCK}$, left) vs. GL261 cells transfected with $NOTCH1$-shRNA vector (GL261-$NOTCH1^{KD}$, right). Right: expanded view of inset regions (white box) in left panel. Insets 1–6, scale bar, 20 μm.

of Notch1, Sox9 and Sox2 in GSCs was detected by immunofluorescent staining (Supplementary Fig. 5). More important, the upregulation of *SOX2* induced by *NOTCH1* overexpression in the non-GSC subpopulation was significantly restored by inhibition of *SOX9* (Fig. 4o,p). These results indicate that *NOTCH1* promotes the transcription of *SOX2* through *SOX9*.

Four putative Sox9-binding sites were identified on the *SOX2* promoter (Fig. 5a). Thus, a set of pGL4-derived constructs were transiently transfected in GBM2 cells (Fig. 5b). All constructs showed activity in these cells, suggesting the presence of the elements necessary for the transcriptional activity of the *SOX2* promoter region. Fragment 1 (−2237 to +111 bp), which harbors all four putative Sox9-binding sites, exhibited the highest luciferase activity. Along with shortening of inserted fragments and a decrease in the number of putative binding sites, the luciferase activity was also subsequently downregulated. Fragment 5, which did not contain any of the putative binding sites, had the lowest luciferase activity, with levels similar to those in the control group (Fig. 5b).

To analyze the in vivo interaction between Sox9 and the putative binding sites, a ChIP assay was performed on the chromatin of GBM2 cells. The antibody to Sox9 precipitated proteins bound in vivo to the amplified DNA sequence harboring three Sox9 putative sites (sites 1–3), whereas no PCR products were observed in the DNA sequence containing site 4 (Fig. 5c).

We next determined whether the binding sites of sites 1–3 were functional using an electrophoretic mobility shift assay (EMSA). Retarded bands were observed in each case using hot (labelled) probes for sites 1–3 (Fig. 5d). We tested the formation of these complexes with an excess of unlabeled specific probes (Fig. 5d), confirming the binding specificity. Moreover, after the administration of an antibody to Sox9, retarded bands were attenuated significantly (Fig. 5d) compared with the control groups (Fig. 5d).

Finally, a deletion analysis was performed to confirm the binding sites. Fragment 6, which was derived from fragment 1 by deletion of sites 1–3, was constructed into pGL4 and then co-transfected with *SOX9* in GBM2 cells. *SOX9* overexpression did not elevate the luciferase activity (Fig. 5e). These data strongly suggest that Sox9 may bind to sites 1–3 in the *SOX2* promoter and upregulate the transcription of the *SOX2* gene.

**Sox2 promotes the GSC distribution by increasing Notch1.** Notably, when we knocked down the expression of *SOX9* in *NOTCH1*-overexpression non-GSCs, the mRNA level of *NOTCH1* was also downregulated, consistent with the decrease in *SOX2* (Fig. 4o). This indicates that Sox2 might be able to regulate the transcription of *NOTCH1*. Thus, we knocked down *SOX2* in the GSCs and overexpressed it in the non-GSC subpopulation. The levels of *NOTCH1* and activation of the Notch signaling pathway were also upregulated and downregulated, respectively, and *SOX2* was correspondingly overexpressed and knocked down (Fig. 6a–d). Taken together, these findings demonstrate a positive-feedback loop between *NOTCH1* and *SOX2*.

Next, we questioned whether knockdown of *NOTCH1* could affect the invasive phenotype of Sox2$^+$ glioma cells. Therefore, we implanted human GBM3 cells into the right striatum adjacent to the corpus callosum in NOD/SCID mice. At 28 d after implantation,

Fig. 4 | *NOTCH1* promotes the transcription of *SOX2* via *SOX9*. a,b, Spatial relationship between Sox2$^+$ cells (red) and nerve fibers (NF200$^+$, green) at the invasive frontier in glioma subjects as detected by immunofluorescence staining. Three subjects, three male, aged from 46–57, three sections per sample, ten high-power fields per section, 450 Sox2$^+$ cells in total. Representative laser confocal microscopy images of nuclei stained with DAPI (blue) are shown. Scale bar, 20 μm (**a**). Quantitative analysis of minimum distance of every Sox2$^+$ cells from nerve fibers in three glioma subjects (**b**). **c**, Correlation between *SOX2* mRNA levels and stemness score. Expression data were derived from glioblastoma (540 data set, Pearson correlation, $n = 540$ biologically independent subjects, two-tailed). **d**, Adherence of GSCs (CD133$^+$) to neurites of neurons cultured in vitro after knocking down *SOX2* expression in GSCs. Data for quantitative analysis were derived from three biologically independent coculture samples, six to eight high-power fields per sample. The data shown are mean ± s.d. A two-sided Student's *t* test was used to generate *P* values ($t = 7.2$, $n = 23$ high-power fields, df = 44). **e**, Correlation between *NOTCH1* and *SOX2* mRNA levels in GSCs (Pearson correlation, $n = 7$ biologically independent subjects, $r = 0.953$, two-tailed, $P = 8.7 \times 10^{-4}$), NSCs (Pearson correlation, $n = 5$ biologically independent subjects, $r = −0.815$, two-tailed, $P = 0.09$) and normal cortex (Pearson correlation, $n = 6$ biologically independent samples, $r = 0.036$, two-tailed, $P = 0.95$). Expression data were derived from GSCs (Pollard data set). **f**, Correlation between *NOTCH1* and *SOX2* mRNA levels in GSCs (Pearson correlation, $n = 30$ biologically independent samples, two-tailed; left) and non-GSCs (Pearson correlation, differentiated glioma cells, $n = 10$ biologically independent samples, two-tailed; right). Expression data were derived from the GSE67089 cohort. **g**, Relative expression of *SOX2* mRNA after knocking down *NOTCH1* in GSCs by siRNA, as detected by rtPCR, $n = 4$ biologically independent samples; data shown are mean ± s.d. A two-sided Student's *t* test was used to generate *P* values, Mock vs. *NOTCH1*^{KD} (GSCs-U87 group, $P1 = 0.085$, df1 = 6, $t1 = 2.1$; $P2 = 0.028$, 2df2 = 6, $t2 = 2.9$; $P3 = 0.017$, df3 = 6, $t3 = 3.3$. GSCs-GBM1 group, $P1 = 0.012$, df1 = 6, $t1 = 3.5$; $P2 = 0.0017$, df2 = 6, $t2 = 5.4$; $P3 = 0.0017$, df3 = 6, $t3 = 5.4$. GSCs-GBM2 group, $P1 = 5.1 \times 10^{-7}$, df1 = 6, $t1 = 22$; $P2 = 1.9 \times 10^{-5}$, df2 = 6, $t2 = 12$; $P3 = 1.1 \times 10^{-4}$, df3 = 6, $t3 = 8.9$). No correction for multiple comparisons was applied. **h**, Protein level of Sox2 after knocking down *NOTCH1* in GSCs by shRNA, as detected by western blotting. Representative results from three replicates are shown. Mock, GSCs transfected with control shRNA; *NOTCH1*^{KD}-1–2, GSCs transfected with *NOTCH1* shRNA 1–2 (**g,h**). **i**, Relative expression of *SOX2* mRNA after overexpressing *NOTCH1* in non-GSCs, as detected by rtPCR, $n = 4$ biologically independent samples; data shown are mean ± s.d. A two-sided Student's *t* test was used to generate *P* values (non-GSCs-U87 group, df = 6, $t = −22$; non-GSCs-GBM1 group, df = 6, $t = −27$; non-GSCs-GBM2 group, df = 6, $t = −13$). No correction for multiple comparisons was applied. **j**, Protein level of Sox2 after overexpressing *NOTCH1* in GSCs, as detected by western blotting. Representative results from three replicates are shown. Vector, non-GSCs transfected with pcDNA3.1 plasmid; *NOTCH1*^{OE}, non-GSCs transfected with pcDNA3.1-*NOTCH1* plasmid (**i,j**). **k,l**, Spatial relationship between Sox9$^+$ cells (red) and nerve fibers (NF200$^+$, green) at the invasive frontier in glioma subjects, as detected by immunofluorescence staining. Three subjects, three male, aged 46–64, three sections per sample, ten high-power fields per section, 440 Sox9$^+$ cells in total. Representative laser confocal microscopy images of nuclei stained with DAPI (blue) are shown. Scale bar, 20 μm (**k**). Quantitative analysis of minimum distance of every Sox9$^+$ cell from nerve fibers in three glioma subjects (**l**). **m**, Correlation between *SOX9* mRNA levels and stemness score. Expression data were derived from glioblastoma (540 data set, Pearson correlation, $n = 540$ biologically independent samples, two-tailed). **n**, Heatmap showing expression levels of *SOX2*, *SOX9* and *NOTCH1* with relative ordering in 540 subjects in the TCGA-540 cohort, ranked by stemness scores. **o**, Relative expression of *SOX2* mRNA following co-interference of *NOTCH1* and *SOX9* in non-GSCs, as detected by rtPCR, $n = 4$ biologically independent samples; data shown are mean ± s.d. A two-sided Student's *t* test was used to generate *P* values, mock vs. *NOTCH1* (non-GSCs-U87 group, $P1 = 2.7 \times 10^{-4}$, df1 = 6, $t1 = 7.6$; $P2 = 4.4 \times 10^{-5}$, df2 = 6, $t2 = 10$; non-GSCs-GBM2 group, $P1 = 1.70 \times 10^{-4}$, df1 = 6, $t1 = 8.259$; $P2 = 1.24 \times 10^{-5}$, df2 = 6, $t2 = 13.065$; $P3 = 3.16 \times 10^{-6}$, df3 = 6, $t3 = 16.50$). No correction for multiple comparisons was applied. **p**, Protein level of Sox2 following co-interference of *NOTCH1* and *SOX9* in non-GSCs, as detected by western blotting. Representative results from three replicates are shown. Mock, non-GSCs transfected with control siRNA; *SOX9*^{KD}-1–2, non-GSCs transfected with *SOX9* siRNA 1–2; *NOTCH1*^{OE}, non-GSCs transfected with the pcDNA3.1-*NOTCH1* plasmid (**o,p**). All full-length western blots are presented in Supplementary Figure 10.

brain tissues were subjected to diffusion tensor imaging (DTI), laser confocal scanning microscopy and Nissl histological staining. The coregistration was based on directly identifiable landmarks (Supplementary Fig. 6). Tumor cells in the control group invaded the contralateral hemisphere and reached the bilateral hippocampus along white matter fibers (such as the corpus callosum and hippocampal projection fibers). Notably, most of these glioma cells were Sox2+ (Fig. 6e–h). After knocking down the expression of *NOTCH1* in GBM3 cells, the invasive phenotype was inhibited significantly (Fig. 6e–h). Taken together, these results show that knockdown of *NOTCH1* inhibits the invasive phenotype of Sox2+ glioma cells along white matter tracts (Fig. 6e–h).
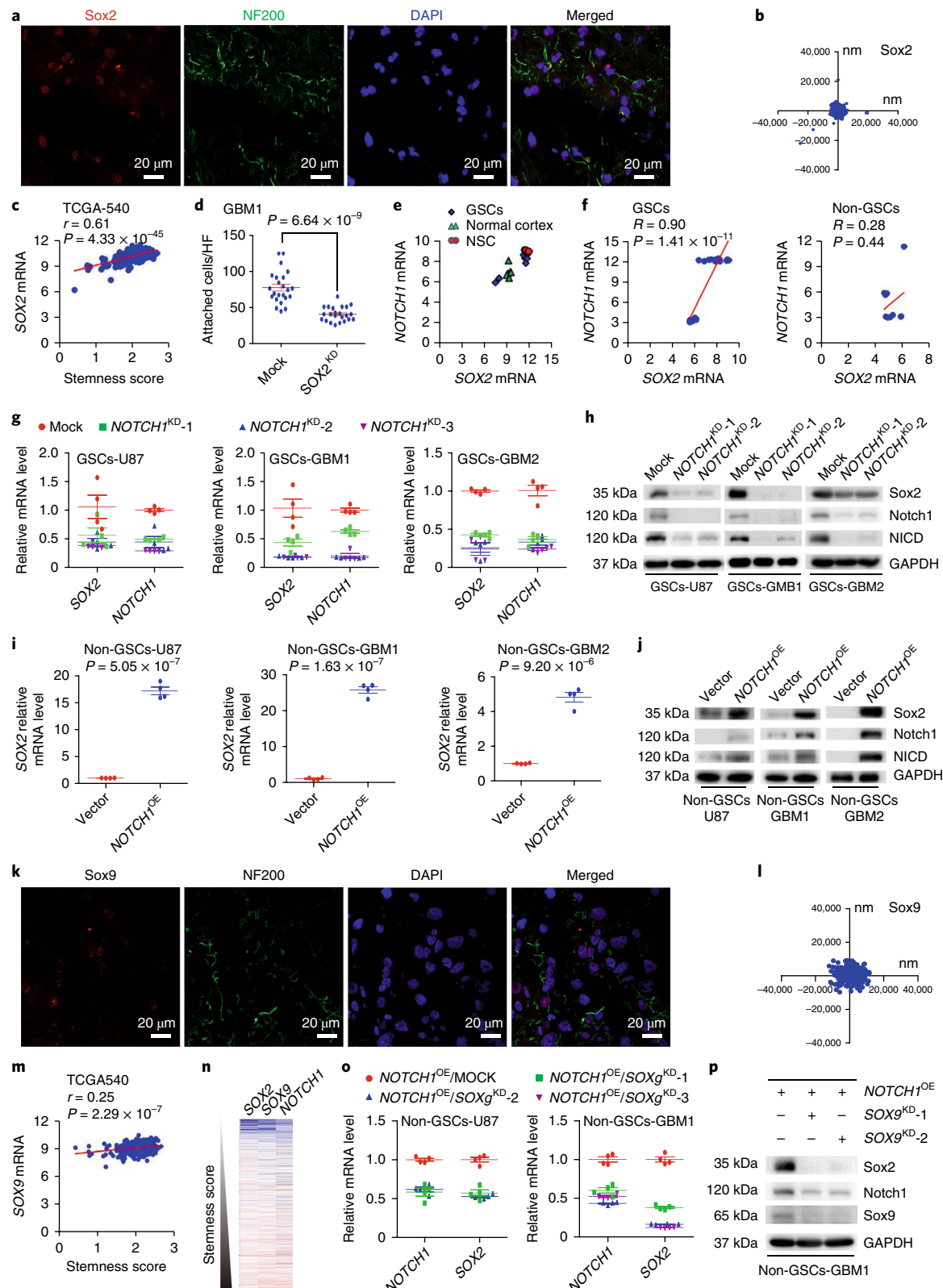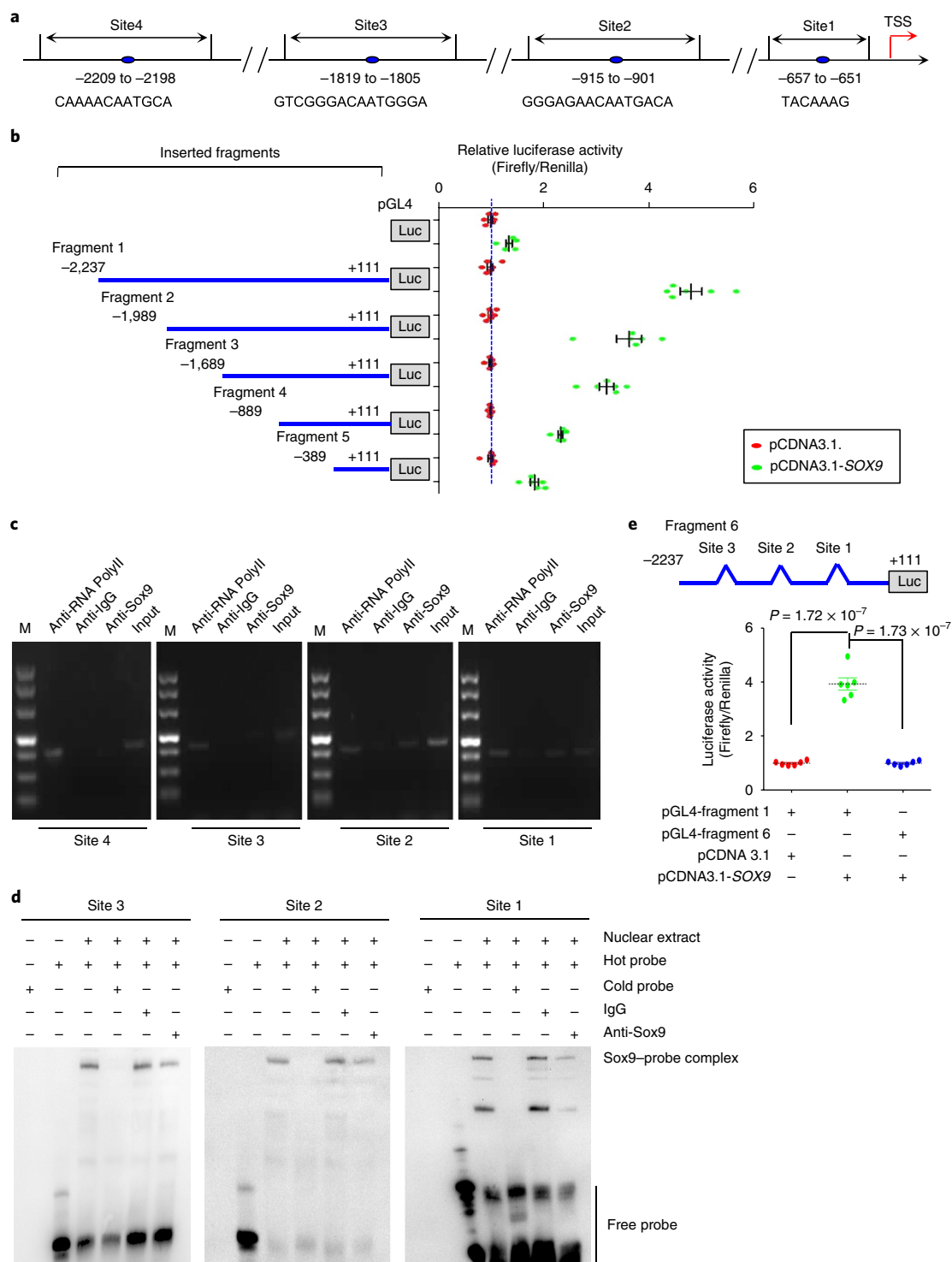
Fig. 5 | Sox9 initiates the transcription of *SOX2* by directly binding to the promoter region of *SOX2*. a, Putative binding sites of Sox9 in promoter region of *SOX2*. TSS, transcriptional start site. **b**, Luciferase reporter assay in GSCs derived from GBM2 cells using different fragments of *SOX2* promoter after transfection with *SOX9*, $n = 6$ biologically independent samples; data shown are mean ± s.d. A two-sided Student's t test was used to generate P values, mock vs. $SOX9^{OE}$ ($P1 = 4.1 \times 10^{-4}$, df1 = 10, $t1 = -5.2$; $P2 = 8.2 \times 10^{-9}$, df2 = 10, $t2 = -17$; $P3 = 1.8 \times 10^{-6}$, df3 = 10, $t3 = -9.9$; $P4 = 5.5 \times 10^{-7}$, df4 = 10, $t4 = -11$; $P5 = 2.1 \times 10^{-8}$, df5 = 10, $t5 = -16$; $P6 = 4.4 \times 10^{-11}$, df6 = 10, $t6 = -30$). **c**, ChIP analysis of GSCs derived from GBM2 cells. PCR primers were designed to surround the predicted Sox9-binding sites 1–4 in the *SOX2* promoter. Nonspecific IgG and anti-RNA polymerase II (anti-RNA PolyII) were used as controls. These experiments were repeated independently three times with similar results. M, DNA ladder. **d**, EMSA with nuclear extracts from GBM2 GSCs. Oligonucleotides corresponding to the predicted Sox9-binding sites 1–3 sequences in the *SOX2* promoter were used in these assays. Additional incubation with an antibody to Sox9 was done to detect a supershifted signal on the gel. These experiments were repeated independently three times with similar results. **e**, Luciferase reporter assay in GSCs derived from GBM2 cells using fragment 6, which carried a deletion of the putative Sox9-binding sites 1–3 of the *SOX2* promoter after transfection with *SOX9*, $n = 6$ biologically independent samples; data shown are mean ± s.d. A two-sided Student's t-test was used to generate P values. ($t1 = -13$, df = 10; $t2 = 13$, df = 10). No correction for multiple comparisons was applied.

Subsequently, we began to unravel the mechanisms responsible for Sox2 regulation of *NOTCH1* transcription. Sox2 can promote the transcription of *notch1* in mouse retinal progenitor cells via an enhancer-dependent model[18]. Moreover, bioinformatics analysis revealed five putative Sox2-binding sites containing thee putative *cis* elements located in the human *NOTCH1* gene (Supplementary Fig. 7a). Thus, different fragments containing three putative *cis* elements were cloned into a minimal promoter of the pGL4 vector, which was transiently co-transfected with *SOX2* into GBM2 cells (Supplementary Fig. 7b). To our surprise, luciferase activity did not increase in any of the groups carrying the inserted putative *cis* elements (Supplementary Fig. 7b). Taken together, these data strongly suggest the presence of an additional mechanism by which *SOX2* upregulates *NOTCH1* transcription in human GSCs.

The *NOTCH1* promoter contains some (G+C)-rich regions (Fig. 7a), and CpG island methylation–mediated epigenetic regulation controls the transcription of this gene[19]. We found that *SOX2* expression was negatively correlated with *NOTCH1* methylation in a microarray data set (Fig. 7b). Then we performed methylated DNA immunoprecipitation (MeDIP) PCR (Fig. 7c,d). We observed that the methylation level in this region was substantially reduced in the *SOX2*-overexpressing GBM2 non-GSC subpopulation (Fig. 7c). When we knocked down the expression of *SOX2* in the GBM2 GSC subpopulation, we observed an elevated methylation level of *NOTCH1* promoter (Fig. 7d), decreased expression of *NOTCH1* (Fig. 7e,f), and downregulated activity of Notch signaling (Fig. 7f). After treatment with 5-Aza, promoter methylation (Fig. 7d), the expression of *NOTCH1* (Fig. 7e,f), and the activation of Notch signaling (Fig. 7f) were restored. These results suggest that the upregulation of *SOX2* in GSCs induces the transcription of *NOTCH1* by decreasing the methylation level of its promoter.

The epigenetic regulatory mechanism of *SOX2* in GSCs has been elucidated recently[20]. This research indicates that multiple cell cycle and epigenetic regulators are transcriptional targets of Sox2. Among them, *TET3* (ten-eleven translocation 3) has a role in the DNA demethylation process[20]. Using the data set GSE15209, we observed that the mRNA level of *NOTCH1* was correlated with the mRNA level of *TET3* in GSCs (Fig. 7g). There was also a positive relationship between the expression of *SOX2* and *TET3* (Fig. 7g). The

upregulation of *NOTCH1* transcription induced by *SOX2* overexpression in the non-GSC subpopulation of GBM2 was significantly restored by the inhibition of *TET3* (Fig. 7h). Moreover, the downregulation of *NOTCH1* promoter methylation induced by overexpressing *SOX2* was also restored by the knockdown of *TET3* (Fig. 7i). These results indicate that Sox2 promotes *NOTCH1* transcription through *TET3*-mediated DNA demethylation. Taken together, these results suggest that there is a reciprocal activation loop between *SOX2* and *NOTCH1* to facilitate GSC distribution along white matter tracts (Supplementary Fig. 8).

SOX2–NOTCH1 loop is a diagnostic or therapeutic target. To determine the significance of the reciprocal loop between *SOX2* and *NOTCH1* in glioma progression, a cohort of 218 glioma subjects from Southwest Hospital and TianTan Hospital was analyzed. There was a positive relationship between Sox2 and Notch1 at the tumor periphery (Fig. 8a,b). Moreover, in the five samples containing the entire tumor center, tumor periphery and distant brain tissue, we found a positive correlation between Sox2 and Notch1 protein levels in these regions, although the highest expression levels of these two proteins were found in the tumor periphery (Fig. 8c). This positive correlation was also present in all 218 subjects (Fig. 8d,e). In addition, the expression pattern of Sox9 in glioma samples was similar to that of Sox2 and Notch1, further validating the positive-feedback loop among Sox2, Sox9 and Notch1 (Supplementary Fig. 9 and Supplementary Table 1). Next, we assessed the clinicopathological significance of these two proteins. Sox2^{hi}Notch1^{hi} subjects showed an advanced age, low Karnofsky performance status score, and high histological grade (Supplementary Table 2). Finally, Kaplan-Meier and univariate Cox proportional hazard regression analyses of 108 glioma subjects (64 high-grade subjects) with prognostic information indicated that high Sox2 and Notch1 expression levels were correlated with a poor prognosis (Fig. 8f–h). The combination of Sox2 and Notch1 expression showed that the cases with Sox2^{hi}Notch1^{hi} had a significantly poorer prognosis (OS, overall survival, 419 d; DFS, disease-free survival, 305 d) compared with the other groups (Sox2^{lo}Notch1^{lo}, OS, 1,710 d; DFS, 1,242 d; Sox2^{lo}Notch1^{hi}, OS, 591 d; DFS, 489 d; Sox2^{hi}Notch1^{lo}, OS, 1,555 d; DFS, 905 d) (Fig. 8h). More important, Sox2^{hi}Notch1^{hi} was shown to be an independent

Fig. 6 | Sox2 promotes *NOTCH1* transcription. a, Relative expression of *NOTCH1* mRNA after *SOX2* overexpression in non-GSCs, as detected by rtPCR, $n = 4$ biologically independent samples; data shown are mean ± s.d. A two-sided Student's t test was used to generate P values (non-GSCs-U87 group, df = 6, $t = -6.3$; non-GSCs-GBM1 group, df = 6, $t = -11$; non-GSCs-GBM2 group, df = 6, $t = -13$). No correction for multiple comparisons was applied. Vector, non-GSCs transfected with the pcDNA3.1 plasmid; *SOX2*[OE], non-GSCs transfected with the pcDNA3.1-*SOX2* plasmid. **b**, Protein level of Notch1 after Sox2 overexpression in non-GSCs, as detected by western blotting. Representative results from three replicates are shown. Vector, non-GSCs transfected with the pcDNA3.1 plasmid; *SOX2*[OE], non-GSCs transfected with the pcDNA3.1-*SOX2* plasmid. **c**, Relative expression of *NOTCH1* mRNA after knocking down *SOX2* in GSCs by shRNA, as detected by rtPCR, $n = 4$ biologically independent samples; data shown are mean ± s.d. A two-sided Student's t test was used to generate P values, mock vs. *SOX2*[KD] (GSCs-U87 group, $P1 = 0.0086$ df1 = 6, $t1 = 3.8$; $P2 = 0.0027$, df2 = 6, $t2 = 4.9$; $P3 = 0.024$, df3 = 6, $t3 = 3.0$; GSCs-GBM1 group, $P1 = 8.2 \times 10^{-6}$, df1 = 6, $t1 = 14$; $P2 = 1.8 \times 10^{-7}$, df2 = 6, $t2 = 27$; $P3 = 7.1 \times 10^{-7}$, df3 = 6, $t3 = 21$; GSCs-GBM2 group, $P1 = 1.6 \times 10^{-6}$, df1 = 6, $t1 = 18$; $P2 = 2.4 \times 10^{-7}$, df2 = 6, $t2 = 26$; $P3 = 2.1 \times 10^{-7}$, df3 = 6, $t3 = 26$). No correction for multiple comparisons was applied. Mock, GSCs transfected with control shRNA; *SOX2*[KD]-1–3, GSCs transfected with *SOX2* shRNA 1–3. **d**, Protein levels of Notch1 and Notch intracellular domain (NICD) after knocking down *SOX2* in GSCs by siRNA, as detected by western blotting. Representative results. These experiments were repeated independently three times with similar results. Mock, GSCs transfected with control siRNA; *SOX2*[KD]-1 and *SOX2*[KD]-2, GSCs transfected with *SOX2* shRNA 1 and 2. **e–h**, Knocking down the expression of *NOTCH1* in human GBM3 cells influences the invasive phenotype of Sox2+ glioma cells 28 d after orthotopic implantation of 1×10^5 GFP-labeled human GBM3 cells into the right striatum adjacent to the corpus callosum in NOD/SCID mice ($n = 3$ independent mice, three male, each group aged 4–5 weeks). Coregistration of whole-slide fluorescence scanner or confocal laser scanning microscopy and histological (Nissl staining) images based on directly identifiable landmarks. Representative figures. Green, glioma cells; red, Sox2+ cells. White arrowhead indicates tumor mass at primary site. Scale bar, 1.0 mm. Second panel from left: expanded view of inset region (white box) shown in left panel. Scale bar, 50 μm (**e**). Quantitative analysis of invasive glioma cells and Sox2+ cells along white matter tracts determined using Image Pro Plus 6.0. Control group (GBM3-*NOTCH1*[Mock]) versus *NOTCH1* knockdown group (GBM3-*NOTCH1*[KD]). Three mice per group, male, three sections per mouse, six high-power fields per section, $n = 54$. Data are presented as mean ± s.d. Nonparametric test was used to generate P values (**f**, Mann–Whitney, two-tailed; **g**, Mann–Whitney, two-tailed) (**f,g**). Co-registration of whole-slide fluorescence scanner or confocal laser scanning microscopy and DTI images based on directly identifiable landmarks. Representative figures. Right: expanded view of inset region (white box) in the fourth panel from left. Scale bar, 500 μm. These experiments were repeated independently at least three times with similar results (**h**). All full-length western blots are presented in Supplementary Figure 10.

predictor for the prognosis (Supplementary Table 3) and high-grade glioma subjects (Supplementary Table 4). Finally, the therapeutic potential of this positive loop was assessed. After treatment with MK-0752, an inhibitor of the Notch signaling pathway, growth and invasion along the white matter tracts of the xenograft were significantly attenuated (Fig. 8i). No significant neurological side effects were observed within 2–8 weeks.

Discussion

In this study, we found that CD133+Notch1+ GSCs were located along Jagged1 expressed white matter tracts, which displayed a demyelinated characteristic, at the invasive frontier of glioma tissues. Axonally expressed Jagged1 activated the Notch signaling pathway in GSCs and then promoted the transcription of *SOX2* via *SOX9*. Conversely, *SOX2* upregulation decreased
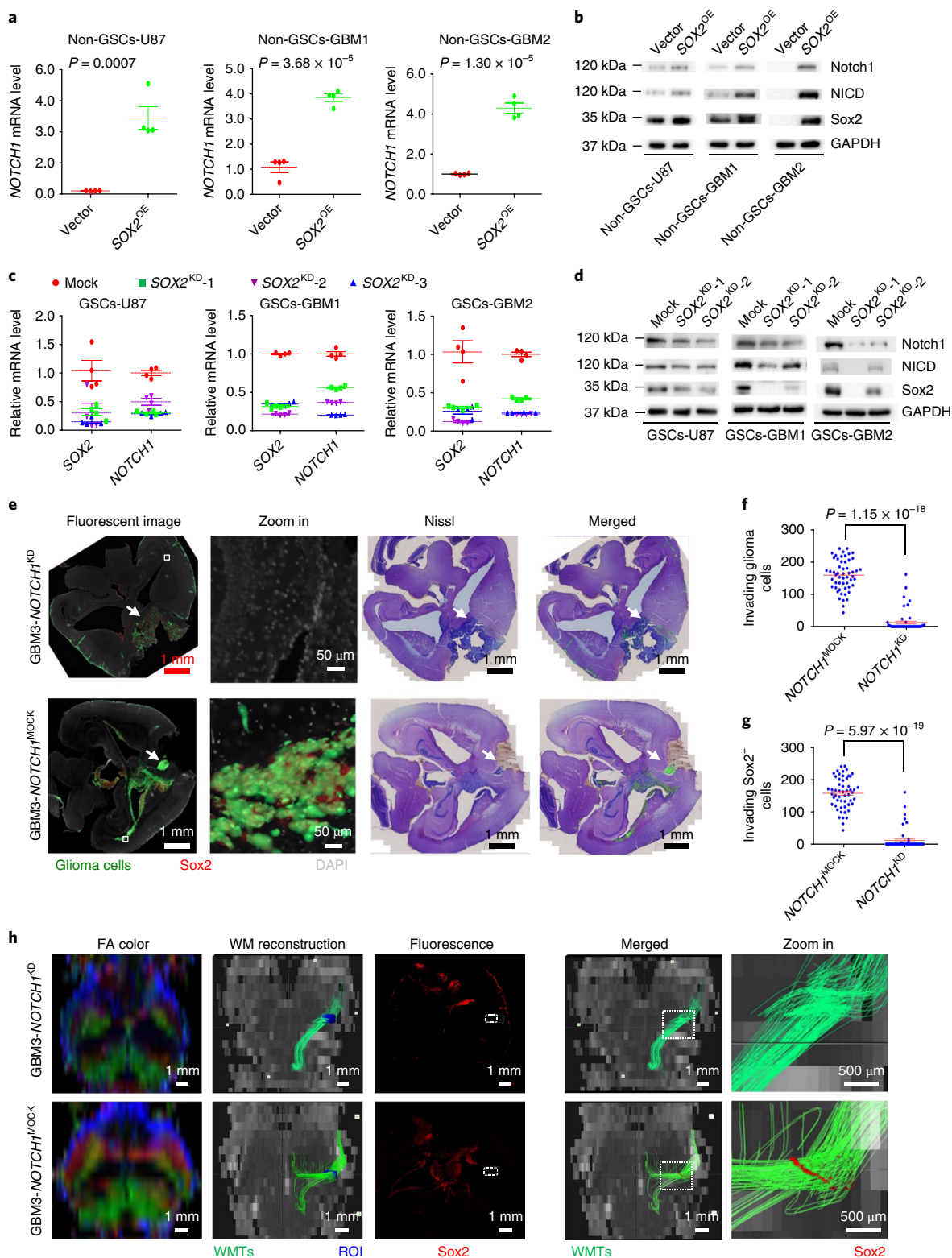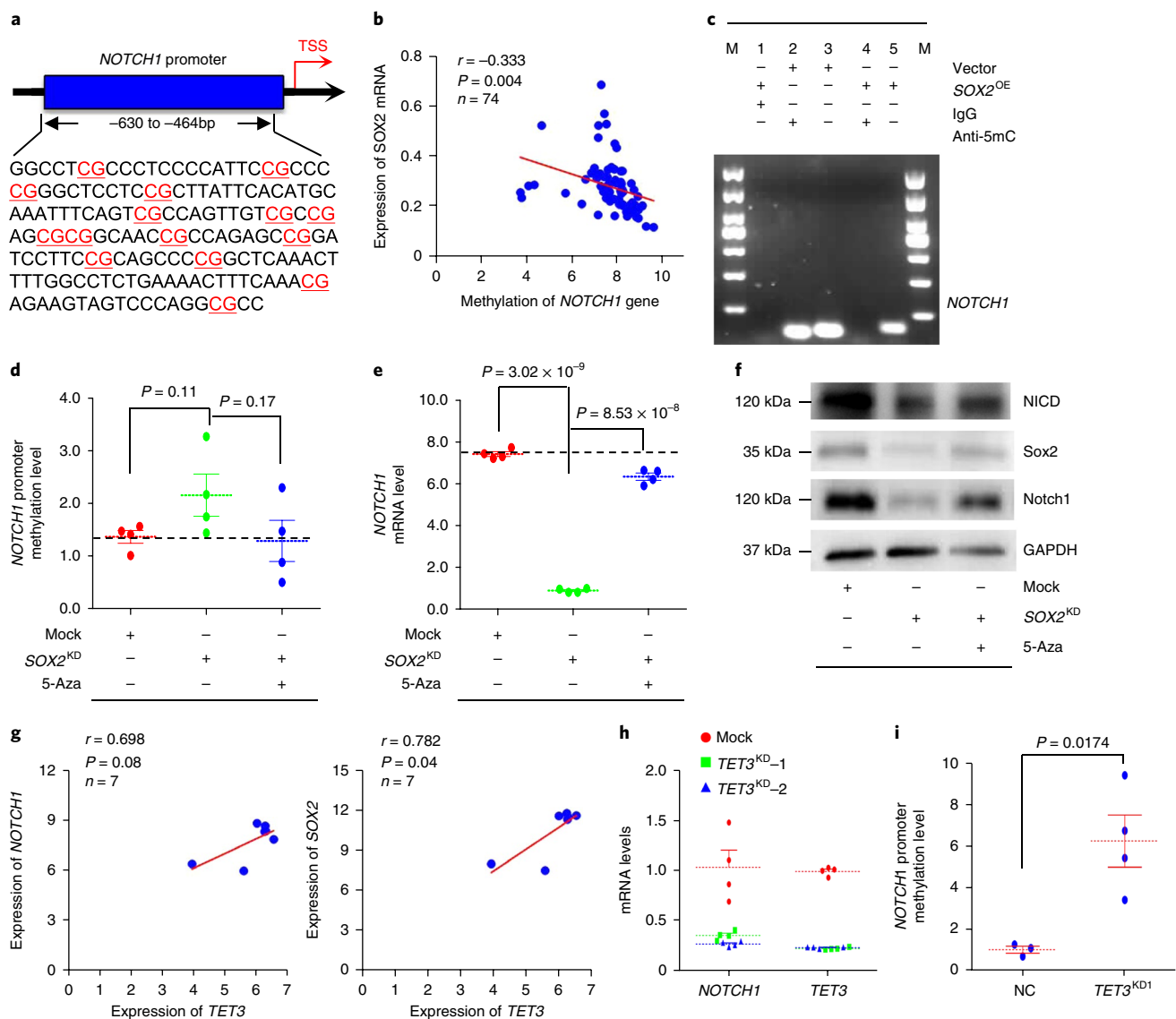
Fig. 7 | Sox2 decreases the methylation level of the *NOTCH1* promoter. a, (G+C)-rich region in the promoter of *NOTCH1* gene. TSS, transcriptional start site. **b**, Correlation between *SOX2* mRNA and methylation level of *NOTCH1* gene. Data were derived from the TCGA (glioblastoma-TCGA-provisional, $n = 74$ biologically independent samples, Pearson correlation, two-tailed). **c**, Methylation of *NOTCH1* promoter after *SOX2* overexpression in GBM2 non-GSC cells, as detected by MeDIP-PCR. Nonspecific IgG was used as a control. These experiments were repeated independently at least three times with similar results. Vector, GBM2 non-GSC cells transfected with pcDNA3.1 plasmid; *SOX2*^OE, GBM2 non-GSCs transfected with pcDNA3.1-*SOX2* plasmid; M, DNA ladder. **d**, Methylation of *NOTCH1* promoter after knocking down *SOX2* in GBM2 GSCs, as detected by MeDIP rtPCR. Nonspecific IgG was used as control, $n = 4$ biologically independent samples, data shown are mean ± s.d., a two-sided Student's *t* test was used to generate *P* values (mock versus *SOX2*^KD, df = 6, $t = -1.9$; SOX2^KD versus SOX2^KD + 5-Aza, df = 6, $t = -1.5$). No correction for multiple comparisons was applied. Mock, GBM2 GSCs transfected with control siRNA; *SOX2*^KD, GBM2 GSCs transfected with *SOX2* siRNA. **e,f**, Expression of *NOTCH1* and NICD after co-interference of *SOX2* (stably overexpressing) or treatment with 5-Aza (1μM for 72h), as detected by rtPCR (**e**, $n = 4$ biologically independent samples, data shown are mean ± s.d.; two-sided Student's *t* test was used to generate *P* values (mock versus *SOX2*^KD, df = 6, $t = 53$; SOX2^KD versus SOX2^KD + 5-Aza, df = 6, $t = 30$) and western blotting (**f**, representative results from three biologically independent experiments; all full-length western blots are presented in Supplementary Figure 10). **g**, Correlation between *NOTCH1* and *TET3* mRNA levels, *SOX2* and *TET3* mRNA levels in GSC (left and right, Pearson correlation, $n = 7$ biologically independent samples, two-tailed). Expression data were derived from GSCs (Pollard data set). **h**, The mRNA levels of *NOTCH1* in GBM2 GSCs after knocking down expression of *TET3* by siRNA, as detected by rtPCR, $n = 4$ biologically independent samples, data shown are mean ± s.d., two-sided Student's *t* test was used to generate *P* values (mock vs. *TET3*-1, $P = 0.0042$, df = 6, $t = 4.5$; mock vs. *TET3*-2, $P = 0.0076$, df = 6, $t = 3.9$). Mock, GBM2 GSCs transfected with control siRNA; *TET*^KD, GBM2 GSCs transfected with *TET3* siRNA. **i**, Methylation of *NOTCH1* promoter after knocking down *TET3* in *SOX2*^OE GBM2 non-GSCs, as detected by MeDIP rtPCR. Nonspecific IgG was used as a control, $n = 3$ (NC group) and $n = 4$ (*TET3*^KD1 group) biologically independent samples, data shown are mean ± s.d., a two-sided Student's *t* test was used to generate *P* values (df = 5, $t = -3.5$). NC, *SOX2*^OE GBM2 non-GSCs transfected with control siRNA; *TET3*^KD, *SOX2*^OE GBM2 non-GSCs transfected with *TET3* siRNA.

the methylation of the *NOTCH1* promoter to reinforce the high expression of *NOTCH1* in GSCs and facilitate their white-matter-tract tropism.

The major principle of neuro-oncological surgery is to attempt to reduce damage to normal nerve function while resecting as much tumor tissue as possible. However, invasion along the periphery of

important white matter fibers can be observed in glioma subjects even at early stages of disease. This pathological feature makes it extremely difficult for neurosurgeons to achieve the above goal and is also an important reason for the high recurrence and poor prognosis of glioma. Based on our study, some molecules in this positive-feedback loop might become drug development targets for the reduction of invasion along white matter fibers; this possibility merits further in-depth studies. Of course, it is difficult to target transcription factors in people with gliomas. Moreover, the benefits of inhibiting the activity of this loop in glioma subjects might far exceed the present finding. Activation of the Notch pathway by the soluble Notch ligand produced by vascular endothelial cells has important roles in the clustered distribution of CSCs along perivascular regions[11]. Therefore, we expect that inhibition of the Notch pathway in GSCs would reduce not only the invasion of these deadly seeds along white matter fibers but also their invasion along perivascular regions. These effects could also explain the clear inhibition of the invasive phenotype of orthotopic xenografts after the suppression of *NOTCH1* expression in GSCs. Recently, researchers have developed a series of Notch pathway inhibitors[21,22]. Clinical studies examining the treatment of glioma using GSI RO4929097 and MK-0752 are ongoing[21,22]. To our surprise, disease conditions were stabilized for >4 months in 24% of glioma subjects who received MK-0752 treatment. Complete remission occurred for an anaplastic astrocytoma subject who achieved complete remission[22]. We also observed that the invasive growth of glioma cells along white matter tracts was significantly inhibited by administration of MK-0752 in our xenograft model. Human NSCs can also migrate along white matter tracts[23,24]. Thus, the mechanism we have mapped in this study may apply to non-neoplastic primitive NSCs but be 'hijacked' by GSCs. However, in completed clinical trials (NCT00803894, NCT00645333, NCT01098344 and NCT01295632), nervous system symptoms were rare in the MK-0752-related toxicities.

Under normal conditions, neuronal axons are wrapped in myelin sheaths. It was previously considered that glioma invasion along white matter tracts emerged in one of two forms: along the outer surface of myelin sheaths and along neuronal axons inside myelin sheaths[25]. However, the myelin sheath surface formed by oligodendrocyte processes does not have the typical components of matrix that support glioma cell migration, such as laminin and collagen[4,26]. Moreover, the myelin sheath surface has some inhibitory molecules[26,27] that exert inhibitory effects on glioma cell migration and proliferation. Although glioma cells can cleave these inhibitory receptors through the secretion of matrix metalloproteinases, ADAMTS5 can also be secreted for extracellular matrix transformation and remodeling that create suitable conditions for glioma cell invasion[4,26,28]. In addition, under the joint action of myosin II

and ion and water channels, glioma cells can change their shape and decrease their volume to traverse the narrow space[4,26,29]. However, these mechanisms explain only how glioma cells can invade white matter fibers; the necessity of this feature remains unknown. Thus, how this specific spatial distribution affects glioma cell has been questioned. Specifically, white matter fibers wrapped in myelin sheaths have been considered unsuitable for glioma cell migration. However, our results show that nerve fibers could express at least some molecules that could promote the expression of GSC stemness transcription factors; for example, Jagged1 activated the Notch pathway to further upregulate the expression of *SOX2*, which is closely associated with stemness maintenance by interacting with the relevant Notch1 receptor on the surface of GSCs. Thus, GSC signals were conducive to survival and stemness maintenance through this spatial distribution, which might be one of the important driving forces by which GSCs invade white matter fibers. In fact, Notch pathway activation also has important roles in the proliferation and stemness maintenance of NSCs[30]. Therefore, GSCs also inherit characteristics similar to those of normal NSCs.

Accordingly, how these GSCs contact nerve fibers in myelin sheaths has been questioned. Our results show that GSCs could adhere to in vitro–cultured, unmyelinated neuronal processes. Belien et al. further support our findings from another angle[28]. In that study, C6 cells were placed at one end of nerve explants and exhibited obvious infiltration and invasion along the longitudinal axis of the unmyelinated optic nerves[28]. Our examination of glioma subject specimens further indicated that some Tau1^{+} or NF200^{+} nerve fibers adjacent to GSCs did not express MBP, suggesting that GSCs might be more prone to distribute along the surface of unmyelinated nerve axons or to enter axons for continuous migration through unmyelinated sites that have been destroyed by glioma. On one hand, this distribution is conducive to a direct interaction between the Notch receptor on the surface of GSCs and the ligand Jagged1 on nerve fibers. On the other hand, this distribution avoids interference by inhibitory molecules on the surface of myelin sheaths. Glioma subjects with extensive demyelination of central nerve fibers are not common[31,32]; however, because myelin sheaths are very sensitive to stimuli, such as ischemia and inflammatory edema[33,34], and because of the extensive edema regions surrounding glioma areas, local destruction of white matter fibers by glioma is very common, especially in high-grade glioma[35,36]. Postoperative radiotherapy also aggravates nerve fiber injury and demyelination changes in areas closely adjacent to glioma[31,32]. These observations provide the structural bases for GSC invasion at the tumor margin along the surface of nerve fibers in areas of edema. Notably, the Jagged1/Notch1 pathway inhibits myelination[13,37,38]. When central myelinated nerve fibers undergo demyelination changes, Jagged1/Notch1 pathway activity is increased[12].

Fig. 8 | Coexpression of Sox2 and Notch1 in glioma is a prognostic predictor of subject outcome. a,b, Immunohistochemical staining of Sox2 and Notch1 expression at the invasive frontier in 27 glioma subjects, 7 female and 20 male, aged 5–64, all containing normal-appearing brain tissue. Immunoreactivity was quantified using Image-Pro Plus software 6.0, one to two sections per subject. The correlation between these two proteins was assessed by Pearson correlation analyses (*n* = 27 biologically independent samples, two-tailed) (**a**). Representative image (**b**). **c,d,** Immunohistochemical staining of Sox2 and Notch1 expression in five glioma subjects, two female and three male, aged 13–63, all containing the tumor center, invasive frontier and distant site. Immunoreactivity was quantified using Image-Pro Plus software 6.0, one to two sections per subject (**c**). Left panel, representative image of whole tumor tissue. Scale bar, 1 mm. Three panels at right, representative images of center (within red line), invasive frontier (within blue line) and distant site (within green line) of the tissue. Scale bar, 50 μm (**d**). **e,** Correlation between Sox2 and Notch1 in 218 glioma subjects. Immunoreactivity was quantified using Image-Pro Plus software 6.0, one to two sections per subject. Correlation of these two proteins was assessed by Pearson correlation analyses (*n* = 218 subjects, two-tailed). **f–h,** Overall and disease-free survival curves of glioma subjects based on immunohistochemical staining data (*n* = 108 subjects, 42 female and 66 male, aged 8–68). Immunoreactivity of Sox2 and Notch1 was quantified using Image-Pro Plus software 6.0 and analyzed by Kaplan-Meier product-limit method and log-rank test. The Youdens index derived from the ROC curve was used to estimate the cutoff value. **i,** Treatment with MK0752 (25 mg.kg⁻¹, twice a week) influences invasive growth along white matter tracts (green) of GL261 GSCs (red) 28 d after orthotopic implantation of 1×10⁵ mCherry-labeled GL261 GSCs into the right striatum adjacent to the corpus callosum in Thy1-EGFP transgenic mice. Three mice per group, male, three sections per mouse, three to six high-power fields per section, *n* = 54 independent high-power fields. Top panels, representative full-slice scanner images of nuclei stained with DAPI (blue). Scale bar, 1 mm. Bottom panels, different regions (white box) of white matter tracts adjacent to hippocampus indicate invading glioma cells (red). Insets 1–4, scale bar, 50 μm.

We examined only a small number of subjects, and the results were insufficient to explain the presence of the extensive demyelination changes in white matter fibers invaded by glioma, which would require in-depth observation with large sample sizes in the future. In addition, based on the high expression of *NOTCH1*, *SOX2* and *CD133* (prominin-1) in the proneural GSCs subtype[39,40], proneural GSCs may be more likely to invade along white matter tracts. Meanwhile, due to the association between radiotherapy and local demyelination of white matter tracts, it should be noted whether the incidence of white matter tract invasion increases in recurrent glioma subjects.

The mechanisms underlying glioma cell invasion along white matter tracts are probably multifactorial[26]. Venkatesh et al. have
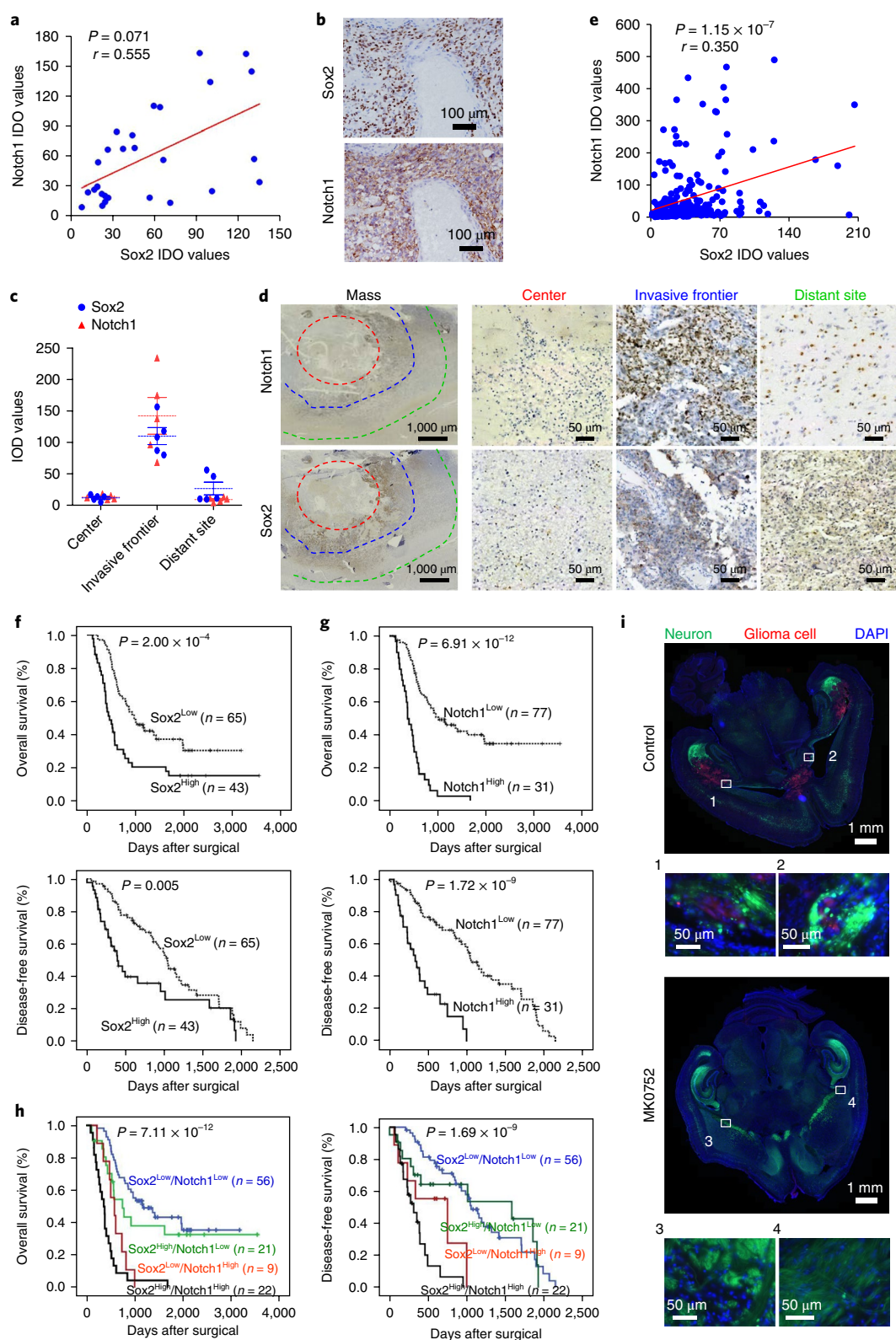
shown that active neurons have an important role in the microenvironment and found that secreted neuroligin-3 promotes glioma growth[41,42]. Thus, this potential role of neural activity and neuroligin-3 in regulating white-matter-tract tropism of GSCs should be investigated in the future. Whether the impairment of nerve fibers or the demyelination status of white matter tracts affects the release of neuroligin-3 and subsequently influences the white-matter-tract tropism of GSCs has been questioned. In addition, the expression levels of integrin α6 (ref. [43]) and integrin α7 (ref. [44]) are elevated in the GSC subpopulation, the extracellular matrix networks between white matter tracts constituted by hyaluronic acid, tenascin R and lecticans might also have an important effect on the invasive phenotype of gliomas[26].

There is a correlation between *NOTCH1* and *SOX2* expression in various tissues and cells[45,46]. Ehm et al. has found that RBP-Jκ interacts with different regions of the mouse NSCs's *sox2* gene promoter to promote its transcription[16]. However, in human stem cells, including GSCs, the specific mechanism underlying the upregulation of *SOX2* expression by the activation of the Notch pathway is not clear. The human *SOX2* gene promoter also has predicted RBP-Jκ-binding sites, and recent studies examining GSCs expressing high epidermal growth factor receptor (*EGFR*) mutant (*EGFRvIII*) have also detected Notch intracellular domain binding in the −1007 to −894 bp region of the *SOX2* gene[47]. Based on these findings, the authors speculate that, similarly to mouse NSCs, *SOX2* transcription is directly upregulated through the binding of RBP-Jκ and the *SOX2* gene promoter in human GSCs[47]. However, we did not detect RBP-Jκ binding in the *SOX2* gene promoter region; in contrast, Sox9 directly interacted with the *SOX2* gene promoter to upregulate *SOX2* transcription. A possible explanation for this difference was that the samples examined by Yin et al. [47] were all GSCs with EGFRvIII, whereas we used GSCs with wild-type EGFR. Using the expression data derived from GSE16011 data set, we found that the positive correlation between *NOTCH1* and *SOX2* was higher in glioma subjects with wild-type EGFR than that in glioma subjects with EGFRvIII mutation. Regarding the relationship between *SOX2* and *SOX9*, previous studies using nervous system tissues have reported a positive correlation between these two factors. Recently, Matheu et al. also discovered a positive correlation between *SOX2* and *SOX9* in GSCs[48]. In this study, we used ChIP, a luciferase reporter gene system, and EMSA to confirm that Sox9 directly transcriptionally regulates *SOX2*.

In summary, GSCs at the brain-tumor interface could interact with the Notch ligand expressed on nerve fibers to reinforce the activation of *NOTCH1-SOX2* feedback loop while simultaneously promoting invasive growth along white matter tracts of these dangerous 'seeds.'

Online content

Any methods, additional references, Nature Research reporting summaries, source data, statements of data availability and associated accession codes are available at https://doi.org/10.1038/s41593-018-0285-z.

References

1. Chen, J., McKay, R. M. & Parada, L. F. Malignant glioma: lessons from genomics, mouse models, and stem cells. *Cell* **149**, 36–47 (2012).
2. Preusser, M., Haberler, C. & Hainfellner, J. A. Malignant glioma: neuropathology and neurobiology. *Wien. Med. Wochenschr.* **156**, 332–337 (2006).
3. Huse, J. T. & Holland, E. C. Targeting brain cancer: advances in the molecular pathology of malignant glioma and medulloblastoma. *Nat. Rev. Cancer* **10**, 319–331 (2010).
4. Cuddapah, V. A., Robel, S., Watkins, S. & Sontheimer, H. A neurocentric perspective on glioma invasion. *Nat. Rev. Neurosci.* **15**, 455–465 (2014).
5. Calabrese, C. et al. A perivascular niche for brain tumor stem cells. *Cancer Cell* **11**, 69–82 (2007).
6. Pietras, A. et al. Osteopontin-CD44 signaling in the glioma perivascular niche enhances cancer stem cell phenotypes and promotes aggressive tumor growth. *Cell Stem Cell* **14**, 357–369 (2014).
7. Bao, S. et al. Glioma stem cells promote radioresistance by preferential activation of the DNA damage response. *Nature* **444**, 756–760 (2006).
8. Singh, S. K. et al. Identification of a cancer stem cell in human brain tumors. *Cancer Res.* **63**, 5821–5828 (2003).
9. Stangeland, B. et al. Combined expressional analysis, bioinformatics and targeted proteomics identify new potential therapeutic targets in glioblastoma stem cells. *Oncotarget* **6**, 26192–26215 (2015).
10. Brown, D. V. et al. Coexpression analysis of CD133 and CD44 identifies proneural and mesenchymal subtypes of glioblastoma multiforme. *Oncotarget* **6**, 6267–6280 (2015).
11. Lu, J. et al. Endothelial cells promote the colorectal cancer stem cell phenotype through a soluble form of Jagged-1. *Cancer Cell* **23**, 171–185 (2013).
12. Stidworthy, M. F. et al. Notch1 and Jagged1 are expressed after CNS demyelination, but are not a major rate-determining factor during remyelination. *Brain* **127**, 1928–1941 (2004).
13. Wang, S. et al. Notch receptor activation inhibits oligodendrocyte differentiation. *Neuron* **21**, 63–75 (1998).
14. Patel, A. P. et al. Single-cell RNA-seq highlights intratumoral heterogeneity in primary glioblastoma. *Science* **344**, 1396–1401 (2014).
15. Gangemi, R. M. et al. SOX2 silencing in glioblastoma tumor-initiating cells causes stop of proliferation and loss of tumorigenicity. *Stem Cells* **27**, 40–48 (2009).
16. Ehm, O. et al. RBPJkappa-dependent signaling is essential for long-term maintenance of neural stem cells in the adult hippocampus. *J. Neurosci.* **30**, 13794–13807 (2010).
17. Candy, P. A. et al. Notch-induced transcription factors are predictive of survival and 5-fluorouracil response in colorectal cancer patients. *Br. J. Cancer* **109**, 1023–1030 (2013).
18. Taranova, O. V. et al. SOX2 is a dose-dependent regulator of retinal neural progenitor competence. *Genes Dev.* **20**, 1187–1202 (2006).
19. Terragni, J. et al. Notch signaling genes: myogenic DNA hypomethylation and 5-hydroxymethylcytosine. *Epigenetics* **9**, 842–850 (2014).
20. Bulstrode, H. et al. Elevated FOXG1 and SOX2 in glioblastoma enforces neural stem cell identity through transcriptional control of cell cycle and epigenetic regulators. *Genes Dev.* **31**, 757–773 (2017).
21. Teodorczyk, M. & Schmidt, M. H. Notching on cancer's door: Notch signaling in brain tumors. *Front. Oncol.* **4**, 341 (2014).
22. Krop, I. et al. Phase I pharmacologic and pharmacodynamic study of the gamma secretase (Notch) inhibitor MK-0752 in adult patients with advanced solid tumors. *J. Clin. Oncol.* **30**, 2307–2313 (2012).
23. Darsalia, V. et al. Cell number and timing of transplantation determine survival of human neural stem cell grafts in stroke-damaged rat brain. *J. Cereb. Blood Flow Metab.* **31**, 235–242 (2011).
24. Aharonowiz, M. et al. Neuroprotective effect of transplanted human embryonic stem cell-derived neural precursors in an animal model of multiple sclerosis. *PLoS One* **3**, e3145 (2008).
25. Giese, A., Bjerkvig, R., Berens, M. E. & Westphal, M. Cost of migration: invasion of malignant gliomas and implications for treatment. *J. Clin. Oncol.* **21**, 1624–1636 (2003).
26. Gritsenko, P. G., Ilina, O. & Friedl, P. Interstitial guidance of cancer invasion. *J. Pathol.* **226**, 185–199 (2012).
27. Iwadate, Y., Fukuda, K., Matsutani, T. & Saeki, N. Intrinsic protective mechanisms of the neuron-glia network against glioma invasion. *J. Clin. Neurosci.* **26**, 19–25 (2016).
28. Belien, A. T., Paganetti, P. A. & Schwab, M. E. Membrane-type 1 matrix metalloprotease (MT1-MMP) enables invasive migration of glioma cells in central nervous system white matter. *J. Cell Biol.* **144**, 373–384 (1999).
29. Beadle, C. et al. The role of myosin II in glioma invasion of the brain. *Mol. Biol. Cell* **19**, 3357–3368 (2008).
30. Yeo, S. Y. & Chitnis, A. B. Jagged-mediated Notch signaling maintains proliferating neural progenitors and regulates cell diversity in the ventral spinal cord. *Proc. Natl Acad. Sci. U.S.A.* **104**, 5913–5918 (2007).
31. Corn, B. W. et al. White matter changes are correlated significantly with radiation dose. Observations from a randomized dose-escalation trial for malignant glioma (Radiation Therapy Oncology Group 83-02). *Cancer* **74**, 2828–2835 (1994).
32. Milic, M. & Rees, J. H. Acute demyelination following radiotherapy for glioma: a cautionary tale. *Pract. Neurol.* **17**, 35–38 (2017).
33. Esiri, M. M. The interplay between inflammation and neurodegeneration in CNS disease. *J. Neuroimmunol.* **184**, 4–16 (2007).
34. Dos Santos, C. D., Picanco-Diniz, C. W. & Gomes-Leal, W. Differential patterns of inflammatory response, axonal damage and myelin impairment following excitotoxic or ischemic damage to the trigeminal spinal nucleus of adult rats. *Brain Res.* **1172**, 130–144 (2007).
35. Sinha, S., Bastin, M. E., Whittle, I. R. & Wardlaw, J. M. Diffusion tensor MR imaging of high-grade cerebral gliomas. *Am. J. Neuroradiol.* **23**, 520–527 (2002).

36. Yen, P. S. et al. White matter tract involvement in brain tumors: a diffusion tensor imaging analysis. *Surg. Neurol.* **72**, 464–469 (2009).
37. Givogri, M. I. et al. Central nervous system myelination in mice with deficient expression of Notch1 receptor. *J. Neurosci. Res.* **67**, 309–320 (2002).
38. Bonini, S. A. et al. Nuclear factor κB-dependent neurite remodeling is mediated by Notch pathway. *J. Neurosci.* **31**, 11697–11705 (2011).
39. Morokoff, A., Ng, W., Gogos, A. & Kaye, A. H. Molecular subtypes, stem cells and heterogeneity: Implications for personalised therapy in glioma. *J. Clin. Neurosci.* **22**, 1219–1226 (2015).
40. Verhaak, R. G. et al. Integrated genomic analysis identifies clinically relevant subtypes of glioblastoma characterized by abnormalities in *PDGFRA*, *IDH1*, *EGFR*, and *NF1*. *Cancer Cell* **17**, 98–110 (2010).
41. Venkatesh, H. S. et al. Neuronal activity promotes glioma growth through neuroligin-3 secretion. *Cell* **161**, 803–816 (2015).
42. Venkatesh, H. S. et al. Targeting neuronal activity-regulated neuroligin-3 dependency in high-grade glioma. *Nature* **549**, 533–537 (2017).
43. Lathia, J. D. et al. Integrin α6 regulates glioblastoma stem cells. *Cell Stem Cell* **6**, 421–432 (2010).
44. Haas, T. L. et al. Integrin α7 is a functional marker and potential therapeutic target in glioblastoma. *Cell Stem Cell* **21**, 35–50.e9 (2017).
45. Zhu, X., Tollkuhn, J., Taylor, H. & Rosenfeld, M. G. Notch-dependent pituitary SOX2(+) stem cells exhibit a timed functional extinction in regulation of the postnatal gland. *Stem Cell Rep.* **5**, 1196–1209 (2015).
46. Phi, J. H. et al. Upregulation of SOX2, NOTCH1, and ID1 in supratentorial primitive neuroectodermal tumors: a distinct differentiation pattern from that of medulloblastomas. *J. Neurosurg. Pediatr.* **5**, 608–614 (2010).
47. Yin, J. et al. Pigment epithelium-derived factor (PEDF) expression induced by EGFRvIII promotes self-renewal and tumor progression of glioma stem cells. *PLoS Biol.* **13**, e1002152 (2015).
48. Garros-Regulez, L. et al. mTOR inhibition decreases SOX2-SOX9 mediated glioma stem cell activity and temozolomide resistance. *Expert Opin. Ther. Targets* **20**, 393–405 (2016).

Author Contributions

J.W. acquired, analyzed and interpreted data and drafted the manuscript. S.L.X., J.J.D. and L.Y. acquired, analyzed and interpreted data. Y.F.G., Y.S., L.L., Z.Y.Y., X.M.L., J.C., H.L.X. and L.Y. acquired data. Y.Q.Z. performed statistical analysis. H.W., J.N.Z., S.Q.L., Q.K.Y., X.J.Y., T.J. and X.Z. analyzed and interpreted data. X.W.B. analyzed and interpreted data, critically revised the manuscript for intellectual content, obtained funding and supervised the study. S.C.Y. initiated the study concept and design, acquired, analyzed and interpreted data, drafted of the manuscript, critically revised the manuscript for intellectual content, performed statistical analysis, obtained funding, and supervised the study. All authors read and approved the manuscript for publication.

Competing interests

The authors declare no competing interests.

Additional information

Supplementary information is available for this paper at https://doi.org/10.1038/s41593-018-0285-z.

Reprints and permissions information is available at www.nature.com/reprints.

Correspondence and requests for materials should be addressed to X.-W.B. or S.-C.Y.

Publisher's note: Springer Nature remains neutral with regard to jurisdictional claims in published maps and institutional affiliations.

Methods

Cell lines, subjects, tumor spheres and GSCs. The human glioma cell line U87 and mouse glioma cell line GL261 were purchased from the American Type Culture Collection.

Paraffin-embedded samples from glioma subjects were obtained during surgery at the Southwest Hospital, Army Medical University (Third Military Medical University) and TianTan Hospital (218 cases between 2005 and 2009; among them, 108 cases had follow-up data). Fifty fresh glioma specimens ($0.5\,mm^3$ in size, derived from within a 200-μm region beyond the macroscopic boundary) were selected from Southwest Hospital, XinQiao Hospital, and DaPing Hospital (between 2012 and 2018). All subjects had sufficient samples for immunohistochemistry. Three samples (GBM1–GBM3) were successfully used for a primary culture. Aborted fetuses were obtained from the Southwest Hospital for neuron cultures. Written informed consent was obtained from all subjects. The Institute Research Medical Ethics Committee of the Army Medical University granted approval for this study.

GSC subpopulations from the U87, GL261 and primary specimens (GBM1–GBM3) were isolated by fluorescence-activated cell sorting and characterized as described[49,50]. Briefly, primary GBM tumors were dissociated with the Papain Dissociation system (Worthington Biochemical). The dissociated tumor cells from U87, GL261 and primary GBMs were recovered in stem cell medium (neurobasal medium (Invitrogen) with B27 supplement (1×, Life Technologies), epidermal growth factor ($20\,ng\,ml^{-1}$, PeproTech) and basic fibroblast growth factor ($20\,ng\,ml^{-1}$, PeproTech)) for 6 h to re-express the GSC surface markers. Cells were then labeled with a P-phycoerythrin-conjugated antibody to CD133 (BD, 566593, 1:100) at 4 °C for 40 min followed by fluorescence-activated cell sorting to isolate the GSCs (CD133^{+}) and non-GSCs (CD133^{−}). The cancer stem cell characteristics were validated by a series of functional assays, including serial tumor sphere formation assay, serum-induced differentiation assay, and in vivo limiting dilution assay, to confirm GSC self-renewal potential, multi-lineage differentiation potency and tumor formation capacity as described[7,49]. Cells were authenticated by examination of their karyotypes and morphologies. All cells were tested for mycoplasma contamination by PCR and verified to be mycoplasma-free.

Published mRNA expression and DNA methylation data sets. The five published mRNA expression data sets (Glioblastoma-TCGA-540; Glioma-French-284, GSE16011; Glioblastoma-TCGA-395; Glioblastoma Stemcells-20, GSE15209 and GSE67089) used in this study were obtained from R2, an Affymetrix analysis and visualization platform developed at the Department of Human Genetics at the Academic Medical Center, University of Amsterdam; this platform included one normal brain, one normal NSC, three glioma, two GSC and one non-GSC data sets (1,279 cases in total). Another microarray data set that contained both the mRNA expression and DNA methylation data (HM450) for glioma subjects was derived from TCGA (Glioblastoma-TCGA-provisional, $n = 74$). Each data set contained the expression profiles of samples with documented genetic and clinical features.

Immunohistochemistry. The glioma tissues were cut into 3-μm-thick sections and processed for immunohistochemistry. The sections were incubated with rabbit monoclonal IgG_1 antibody to Notch1 (Cell Signaling Technology, 3608) at 1:200, rabbit monoclonal IgG_1 antibody to Sox2 (Cell Signaling Technology, 3579) at 1:200, and rabbit polyclonal antibody to Sox9 (Abcam, ab3697) at 1:200 and were stored overnight at 4 °C. Immunostaining was performed with the Envision System using diaminobenzidine (Dako). As a negative control, the primary antibody was replaced with PBS. The expression levels of both proteins were quantified using Image-Pro Plus software 6.0. The antibody information and validation are shown in Supplementary Note.

Immunofluorescent staining, whole-slide fluorescence scanner and laser confocal scanning microscopic analysis. The glioma subject samples were cut into 5-μm-thick sections, fixed with ice acetone and incubated with antibodies to CD133/1 (mouse monoclonal IgG_1, BD, 566593; mouse monoclonal IgG_1, Boster, BM3141; rabbit monoclonal IgG_1, Boster, PB0168) at 1:100; Notch1 (rabbit monoclonal IgG_1; Cell Signaling Technology, 3608) at 1:100; Jagged1 (rabbit monoclonal IgG_1; Cell Signaling Technology, 8658) at 1:100; CDC6 (rabbit polyclonal, Boster, BA1726-1) at 1:100; PBK (rabbit polyclonal, Boster, PB0345) at 1:100; Sox9 (rabbit polyclonal, Abcam, ab3697) at 1:100; CD44 (rabbit polyclonal, Boster, A00052) at 1:100; NF200 (mouse monoclonal, Boster, BM0100) at 1:100; Sox2 (rabbit monoclonal IgG_1; Cell Signaling Technology, 3579) at 1:100; MBP (rabbit polyclonal, Boster, BA0094) at 1:100; or Tau1 (mouse monoclonal IgG1; Merck, MAB3420A4) at 1:100. The appropriate secondary antibodies (Alexa Fluor 546 goat anti-rabbit IgG, A-11010; Alexa Fluor 488 goat anti-mouse IgG, A-11001; Alexa Fluor 647 Goat anti-mouse IgG, A-21236; Alexa Fluor Plus 647 goat anti-rabbit IgG, A32733; Molecular Probes, Invitrogen) were used at 1:1,000. The cells were counterstained with 4,6-diamidino-2-phenylindole (DAPI, Sigma) to reveal nuclei and detected using a whole-slide fluorescence scanner (Axio Scan.Z1, Zeiss) or laser confocal scanning microscopy (Leica SP-5). The immunofluorescence images were imported into Image-Pro Plus 6.0 software for further analysis. To assess the distance between nerve fibers (Tau1^{+} or NF200^{+}) and GSCs (CD133^{+}, Notch1^{+}, Sox2^{+}, Sox9^{+}, CDC6^{+}, PBK^{+} or CD44^{+}) or Jagged1^{+} signals, a nerve fiber

(Tau1^{+} or NF200^{+}) and its adjacent GSC nucleus or Jagged1^{+} signal were randomly labeled by manual processing. Briefly, random selection of GSC marker–positive cells and the nearest nerve fibers was performed. The coordinate values ($X1$, $Y1$) and ($X2$, $Y2$) were obtained using the measurement function in the software. The distance between the GSCs and nerve fibers was calculated using the formula $(X, Y) = (X1 - X2, Y1 - Y2)$ in the picture. Finally, the actual distance was calculated from the scale of the picture. The X-Y coordinate values and the difference between them were calculated and recorded. Then the ratio for the image and the actual distance derived from the confocal ruler were multiplied to obtain the actual distance between nerve fibers (Tau1^{+} or NF200^{+}) and the GSCs or Jagged1^{+} signal. To assess the correlation and overlap coefficients of CD133/Notch1 and MBP/Tau1 protein, Colocalizer Pro for Mac (version 3.0.2) was used to calculate Pearson's correlation coefficient (Rr), Mander's overlap coefficient (R), overlap coefficients ($k1$ and $k2$), and colocalization coefficients ($m1$ and $m2$). The antibody information and validation are shown in Supplementary Note.

The mouse xenograft samples were cut into 5-μm-thick sections and then fixed with ice-cold acetone. The cells were counterstained with DAPI to reveal the nuclei and detected using a whole-slide fluorescence scanner or laser confocal scanning microscopy. The fluorescence images were imported into Image-Pro Plus 6.0 software for further analysis. The fluorescent signals were randomly labeled by manual processing to count the number of satellite lesions adjacent to white matter tracts.

The cultured cell samples were counterstained with DAPI to reveal the nuclei and detected using laser confocal scanning microscopy.

Nissl staining. After immunofluorescent staining and whole-slide fluorescence scanning or laser confocal scanning microscopic analysis, the mouse xenograft tissue sections were immersed in Nissl stain (C0117, Beyotime Biotechnology) for 30 min followed by 95% alcohol for 10 min. After drying at 37 °C, tissue sections were directly sealed with water-based sealing agent. This stain was chosen because of the need to identify cell body positions in histology to perform image registration. Histological images were attained using a whole-slide histological scanner (Axio Scan.Z1, Zeiss) and processed with software (Image-Pro Plus software 6.0).

Diffusion tensor imaging acquisition and three-dimensional reconstruction. Diffusion tensor imaging detection of glioma subjects was performed using a single-shot echo-planar sequence with an acceleration factor of 2 and the following parameters: TR (time of repetition), 3,100 ms; TE (time of echo), 90 ms; FOV (field of view), 250×250 mm; matrix, 192×192; section thickness, 5 mm; interslice gap, 1.5 mm; bandwidth, 1,346 kHz; EPI (echo planar imaging) factor, 128; echo spacing, 0.83; flip angle, 90°; NEX (number of excitation), 3; diffusion encoding in 12 different directions; and b values, 0 and $1,000\,s\,mm^{-2}$. A three-dimensional (3D) model of human DTI was reconstructed using the Strealth Viz Work station of the Stealth Station S7 surgical navigation system (Medtronic).

DTI detection of mouse xenograft was performed with a four-shot spin-echo echo planar imaging sequence, an encoding scheme of 30 gradient directions homogenously distributed on the unit sphere and the following parameters: TR/TE, 3,000 ms/26 ms; FOV, $25\,mm \times 25$ mm; slice thickness, 0.5 mm; matrix size, 128×128; Δ, 12 ms; δ, 4.5 ms; two b values (0 and $800\,s\,mm^{-2}$); and four averages. All image volumes were corrected for head movement and eddy current distortions using FMRIB's Diffusion Toolbox within FSL (http://www.fmrib.ox.ac.uk/fsl). A multivariate linear fitting algorithm was introduced to estimate the diffusion tensor of each voxel, which was then diagonalized to obtain its eigenvalues. For each mouse, fractional anisotropy then was reconstructed for fiber tracking. Whole-brain diffusion tensor reconstruction and tractography were performed in native diffusion space for each mouse using the Diffusion Toolkit (http://trackvis.org/dtk/). Diffusion tensor tractography was calculated using the fiber assignment by the continuous tracking (FACT) method algorithm with criteria that path tracing proceeded until either the fractional anisotropy was <0.2 or the angle between the current and the previous path segment exceeded 35°. An experienced neuroradiologist (S.-C.Y.) manually delineated the region of interest (ROI) near the corpus callosum with the results of immunofluorescence as reference on ADC (apparent diffusion coefficient) images using MRIcron (http://www.mccauslandcenter.sc.edu/mricro/mricron/). The delineated ROI fiber reconstruction images were obtained using TrackVis (http://trackvis.org/dtk/).

The measured water diffusion is fitted to a simple tensor model with a 3×3 symmetrical matrix from which three eigenvalues ($\lambda 1$, $\lambda 2$ and $\lambda 3$) and corresponding eigenvectors ($v1$, $v2$, and $v3$) can be computed. Fractional anisotropy (FA), mean diffusivity (MD), axial diffusivity (DA), and radial diffusivity (DR) are the most commonly used ones, which are defined by the following equations:

$$FA = \sqrt{\frac{1}{2}} \frac{\sqrt{(\lambda_1 - \lambda_2)^2 + (\lambda_2 - \lambda_3)^2 + (\lambda_1 - \lambda_3)^2}}{\sqrt{\lambda_1^2 + \lambda_2^2 + \lambda_3^2}}$$

$$MD = \frac{\lambda_1 + \lambda_2 + \lambda_3}{3}$$

$$DA = \lambda_1$$

$$DR = \frac{\lambda_2 + \lambda_3}{2}$$

After the acquisition of raw data, all the DTI data were processed by ParaVision 6.0.1 software. For the statistical analysis, an independent two-sample t-test was used to compare the differences between *NOTCH1*-knockdown mice and controls with a significant level of $P < 0.05$ (uncorrected, cluster size >10) in each DTI-related measurement (FA, MD, DA and DR).

Coregistration of Nissl, immunofluorescent and DTI images. Based on directly identifiable landmarks observed by either whole-slide fluorescence scanner or confocal laser scanning microscopy and Nissl histological images, coregistration was performed using Adobe Photoshop CS3 Extended software. The numbers of invaded cells were quantified using Image-Pro Plus software 6.0.

To coregister DTI findings with histology results, brain tissues were collected and perfused brain tissue from *NOTCH1*-knockdown mice and controls were prepared for immunofluorescent staining. Briefly, mice were perfused with physiological saline through the right ventricle (~5.8 r.p.m., 10 min) after being anesthetized. After the extremities, liver and tongue turned white, physiological saline was replaced with 4% paraformaldehyde (PFA) for perfusion at a lower flow rate (~4.8 r.p.m., 20 min). After perfusion, brains were carefully excised and post-fixed in 4% paraformaldehyde for 24 h followed by 30% sucrose in PBS for dehydration. After brain tissues were frozen, they were embedded in optimal cutting temperature compound and transverse cut at 30 µm thick for immunofluorescent staining. All sections were blocked in 1% BSA for 1 h at room temperature to prevent nonspecific binding and to increase permeability of antibodies. Sections were then incubated with monoclonal antibody to Sox2 (1:100; CST) at 4 °C overnight. After rinsing, goat anti-rabbit IgG conjugated with Alexa 555 (1:1,000; Invitrogen) was applied for visualization of immunoreactivity. Sections were covered in water-based tablet with Hoechst 33258 (Beyotime). Histological slides were examined with a plan-apochromat 20×/0.8 M27 (ZEISS) fluorescence microscope, and images were captured with a HV-F202SCL (Hitachi) camera using ZEN software (ZEISS). After the images were captured, immunofluorescent images and DTI ROI fiber reconstruction images were imported into Adobe Photoshop CS3 software. The same ROI regions as those in the DTI ROI fiber reconstruction images were delineated in the immunofluorescent images. The Sox2$^+$ tumor cells were extracted by color-range selection, and positively stacked with the original DTI fiber reconstruction images. The antibody information and validation are shown in Supplementary Note.

Adherence assay. Neurons from aborted fetuses were cultured in appropriate culture medium. On the day of the experiment, 100-µl cell suspensions of different GBM2 subpopulations (1×10^5 cells ml^{-1}) were seeded into the same culture plate with neurons, and the dishes were flicked gently to allow all glioma cells to contact the neurons. After incubation in a 5% CO_2 humidified incubator at 37 °C for 5 min, the supernatant and nonadherent glioma cells were discarded. The adherent glioma cells on the neurons were observed and counted under a high-power field microscope.

Migration assay. The different subpopulations derived from GBM2 cells were cultured in the appropriate culture medium. On the day of the experiment, 200-µl cell suspensions (2×10^5 cells ml^{-1}) were seeded onto the top chamber of a 24-well micropore polycarbonate membrane filter with 12.0-µm pores (Becton Dickinson) in serum-free DMEM/F12 culture medium. The bottom chamber was filled with neuronal culture medium as a chemoattractant. After 24 h of incubation in a 5% CO_2 humidified incubator at 37 °C, the membranes were fixed and stained with crystal violet, and the cells on the upper surface were carefully removed with a cotton swab. The migrating cells on the lower surface were observed and counted under a high-power field microscope.

Real-time PCR. Total RNA was isolated from different groups of cells and samples. After reverse transcription, real-time PCR (rtPCR) was performed using the SYBR PrimeScript PCR kit II (TaKaRa). Enrichment of methylated DNA fragments and DNA fragments immunoprecipitated with an antibody to Sox9 in different groups of cells were also determined by rtPCR using the same kit. Glyceraldehyde-3-phosphate dehydrogenase (GAPDH) served as an internal control. The primer sequences, product sizes and annealing temperatures are in Supplementary Table 5.

Western blotting. Equivalent amounts of protein were obtained with an NE-PER Nuclear/Cytosol Extraction Kit (Thermo Scientific) and subjected to western blot analyses. Primary antibodies were used according to the manufacturer's instructions at the following dilutions: rabbit polyclonal anti-GAPDH (Cell Signaling Technology, 2118) at 1:1,000; rabbit monoclonal anti-Notch1 (Cell Signaling Technology, 3608) at 1:1,000; rabbit monoclonal anti-Sox2 (Cell Signaling Technology, 3579) at 1:1,000; mouse monoclonal anti-Sox2 (BOSTER, BM2014) at 1:100; mouse monoclonal anti-Sox9 (Thermo, MA5-17177) at 1:1,000; rabbit monoclonal anti-Sox9 (Abcam, ab3697) at 1:1,000; and rabbit polyclonal anti-Cleaved-Notch1 (Cell Signaling Technology, 4147) at 1:1,000. After incubation with horseradish peroxidase–labeled secondary antibodies, chemiluminescence (SuperSignal West Pico, Pierce) was quantified with Image Lab 4.0. The antibody information and validation are shown in Supplementary Note.

Plasmids, small interfering RNA, oligonucleotides and methylation inhibitors. Full-length human *NOTCH1*, *SOX2* and *SOX9* in the pCMV6 vector were purchased from Origene and then cloned into the BamHI and XhoI restriction sites of the pcDNA 3.1 vector (Invitrogen) for the overexpression assay. pLVshRNA-eGFP expression vector (VL3101) was purchased from Inovogen. pSicoR-mCh-empty vector (Addgene, plasmid 21907) was a gift from Miguel Ramalho-Santos. psPAX2 (Addgene, plasmid 12260) and pMD2.G (Addgene, plasmid 12259) vectors were gifts from Didier Trono. For the promoter assay, the different fragments of the *SOX2* 5′-promoter (fragment 1, −2237 to +111 bp; fragment 2, −1989 to +111 bp; fragment 3, −1689 to +111 bp; fragment 4, −889 to +111 bp; fragment 5, −389 to +111 bp) were amplified by PCR from human genomic DNA. These fragments were then inserted into the pGL4-luc2P vectors (Promega) at the KpnI and HindIII or XhoI and HindIII sites. The sequences of the small interfering RNA (siRNA) and short hairpin RNA (shRNA) are in Supplementary Table 6. Transient transfection of the expression constructs and siRNA was performed 24 h after seeding using different transfection reagents (Effectene, QIAGEN; X-treme GENE HP DNA, Roche; Lipofectamine 2000, Invitrogen) according to the manufacturers's instructions. Stable cell lines were selected with the appropriate antibiotics for at least 48 h after transfection. The DNA methylation inhibitor 5-aza-2′-deoxycytidine (5-Aza, Sigma) was used to treat different groups of cells at a concentration of 1 µM for 72 h.

Site-specific deletion. According to the manufacturer's instructions, *SOX2*-SIE was deleted from fragment 1 (−2237 to +111 bp) to generate fragment 6 using the QuickChange site-directed mutagenesis system (Invitrogen). The site-specific deletion was verified by DNA sequencing.

Luciferase assay. Cells were plated in 24- or 48-well plates 24 h before transfection. All plasmids containing different fragments of the *SOX2* promoter (fragments 1–6) constructed from the pGL4-luc2 vector were co-transfected with a control Renilla luciferase plasmid (pRL-TK). The ratio of experimental plasmid to control plasmid was 50:1. Luciferase assays were performed with the Dual-Luciferase Reporter Assay system (Promega). Briefly, at 24–48 h after transfection, cell lysates were prepared by incubating the cells with 1× passive lysis buffer for 15 min at room temperature. Cell lysates were transferred in triplicate to 96-well plates and analyzed on a Skanlt software 3.2 (Thermo Scientific) according to the manufacturer's instructions. The firefly luminescence signal was normalized to the Renilla luminescence signal.

Chromatin immunoprecipitation assay. Chromatin immunoprecipitation assays were performed according to the protocol provided by Thermo (Bedford). In brief, different vector-transfected GBM2 non-GSC cells were cross-linked with formaldehyde, and cross-linked chromatin was sonicated followed by immunoprecipitation with anti-IgG (Bioward, BD0049) at 1:100, mouse monoclonal anti-RNA polymerase II, mouse monoclonal anti-RBP-Jκ (Santa Cruz Biotechnology, sc-55019) at 1:100, and rabbit monoclonal anti-Sox9 (Abcam, ab3697) at 1:100. After the ChIP assay was performed, the DNA sample was purified and amplified by PCR using the primers listed in Supplementary Table 5. The antibody information and validation are shown in Supplementary Note.

Electrophoretic mobility shift assay. Nuclear extracts were prepared with NE-PER Nuclear and Cytoplasmic Extraction reagents (Thermo). The wild-type and mutant oligonucleotides were labeled with biotin and used as probes. In competition experiments, 100-fold excess oligonucleotides, including *SOX2*-SIE, high-affinity SIE (hSIE) and irrelevant fosintragenic regulatory element (FIRE) were used (Supplementary Table 6). For the supershift experiment, nuclear extracts were preincubated with mouse monoclonal anti-Sox9 (Thermo, MA5-17177) at 1:25, and an IgG (Bioward, BD0049) at 1:25 antibody was used as a negative control. Protein–DNA complexes were detected using the Light Shift Chemiluminescent EMSA kit (Thermo). Antibody information and validation are shown in Supplementary Note.

Methylated DNA immunoprecipitation. Chromatin was isolated from ~1×10^6 cells and sonicated with a sonicator (Diagenode). To perform MeDIP, sonicated chromatin was incubated overnight with a goat anti-human antibody to 5-methlcytidine and subsequently for 2 h with rabbit anti-goat IgG-coupled magnetic beads at 4 °C. After elution, the methyl DNA was purified. One pair of primers (Supplementary Table 5) was designed to amplify the potential methylated region in the *NOTCH1* promoter (−630 to −464 bp). Enrichment of methylated DNA fragments obtained from the MeDIP assay was determined by PCR or rtPCR with the SYBR PrimeScript PCR kit (TaKaRa). Antibody information and validation are shown in Supplementary Note.

Orthotopic tumor induction in the brain. NOD/SCID mice were purchased from the animal center (Army Medical University), and Thy1-EGFP transgenic mice were a gift from Zhen-Ge Luo. All mice were treated according to the guidelines of the Army Medical University animal committee. The 1×10^5 green fluorescent protein (GFP)-labeled GSCs derived from GBM2 and GBM3 cells were suspended in 2 µl of PBS and then injected orthotopically into the right striatum adjacent to

the corpus callosum of 4-week-old female NOD/SCID mice. Four independent groups of animals ($n = 5$ per group) were assessed: mice implanted with *NOTCH1*-shRNA-transfected GSCs; mice implanted with vector-transfected GSCs; mice implanted with wild-type GSCs and treated with PBS; and mice implanted with wild-type GSCs and treated with MK-0752. The 1×10^5 mCherry-labeled GSCs derived from GL261 cells were injected at the same site of 4-week-old female Thy1-EGFP transgenic mice to construct another xenograft model. Four independent groups of animals ($n = 5$ per group) were assessed: mice implanted with *NOTCH1*-shRNA-transfected GSCs and killed at 2 weeks after injection; mice implanted with *NOTCH1*-shRNA-transfected GSCs and killed at 4 weeks after injection; mice implanted with vector-transfected GSCs and killed at 2 weeks after injection; and mice implanted with vector-transfected GSCs and killed at 4 weeks after injection. The tumors were examined using a magnetic resonance imaging system and then DTI acquisition. At 2 weeks (GL261-implanted mice) and 4 weeks (GL261, and GBM3-implanted mice) after injection, tumor-bearing tissues, which were obtained from the mice transplanted with the cells from different groups, were fixed with 4% paraformaldehyde and cut horizontally into 5-µm sections using a Vibratome. The sections were mounted on slides and then subjected to immunofluorescent and Nissl staining. Images were captured using a whole-slide fluorescence scanner (Axio Scan.Z1, Zeiss) and a Leica DMRE microscope (Leica Microsystems).

Statistical analyses. Statistical analyses were performed using the SPSS statistical software package (standard version 16.0). Measurement data are presented as mean ± s.d. Animals from different cages in the same experimental group were selected to assure randomization. Animals and cultures were randomly assigned for drug treatment and transduction with different constructs. The investigators were blind to group allocation during data collection and analysis, including immunohistochemistry, immunofluorescent staining and DTI, but not during survival analysis. No animals or data points were excluded from the analyses. Data distribution was assumed to be normal but this was not formally tested.

The measurement data from rtPCR, immunofluorescent staining, tumor sphere formation assay, adherence assay, migration assay, DTI detection and immunohistochemistry were analyzed using Mann-Whitney and Student's t-test. Differences were considered significant at $P < 0.05$.

Correlations between the expression (mRNA or protein) of *CD133* and *NOTCH1*, Notch receptors and *SOX2*, NTFs and *SOX2*, *NOTCH1* and *TET3*, *SOX2* and *TET3*, between the mRNA expression of *SOX2* and the stemness score, *SOX9* and the stemness score, *NOTCH1* and the stemness score, and between the mRNA expression of *SOX2* and the promoter methylation of *NOTCH1* were assessed by Pearson correlation analyses. Correlation of *SOX2*, *SOX9* and *NOTCH1* mRNA

expression was assessed with Kendall's tau-b analysis. Correlation between Notch1 and Sox2 protein coexpression and the clinicopathological features of glioma subjects was analyzed with the χ^2 test or Fisher's exact test. Pearson's correlation coefficient (Rr), Mander's overlap coefficient (R), overlap coefficients ($k1$ and $k2$) and colocalization coefficients ($m1$ and $m2$) to describe the correlation between the Tau1$^+$ signal and the CD133$^+$ or Jagged1$^+$ signal were calculated using Colocalizer Pro for Mac (version 3.0.2).

An estimated survival events analysis would be needed to provide 70% power for a log-rank test, corresponding to survival rate of 0.4 versus 0.1, with a two-sided α of 0.05. Survival curves were estimated according to the Kaplan-Meier product-limit method, and the differences between the survival curves were assessed with the log-rank test. Cut-off values of Sox2 and Notch1 expression were determined by the Youden index using the bootstrap-adjusted AUROC metric. Univariate survival analysis was performed using the Kaplan-Meier and Cox proportional hazards (CPH) models, with comparisons performed using Mantel-Cox log-rank tests. For multivariate analyses based on CPH models, the covariates for CPH models included Sox2 and Notch1 expression as well as established risk factors, including sex, age at surgery, Karnofsky performance status score and histological grade, all of which were dichotomized to assess the predictions of OS and DFS. The P value was calculated using the two-sided Wald test.

Reporting Summary. Further information on experimental design is available in the Nature Research Reporting Summary linked to this article.

Data Availability

All routine analysis methods are included in Methods. The data that support the findings of this study are presented in the paper and supplementary materials and all raw data are available from the corresponding author upon reasonable request. The five published mRNA expression data sets (Glioblastoma-TCGA-540; Glioma-French-284, GSE16011; Glioblastoma-TCGA-395; Glioblastoma Stemcells-20, GSE15209 and GSE67089) used in this study were obtained from R2, an Affymetrix analysis and visualization platform developed at the Department of Human Genetics at the Academic Medical Center, University of Amsterdam.

References

49. Yu, S. C. et al. Isolation and characterization of cancer stem cells from a human glioblastoma cell line U87. *Cancer Lett.* **265**, 124–134 (2008).
50. Zhou, W. et al. Periostin secreted by glioblastoma stem cells recruits M2 tumour-associated macrophages and promotes malignant growth. *Nat. Cell Biol.* **17**, 170–182 (2015).

nature research

Corresponding author(s): Shi-Cang Yu, Xiu-Wu Bian

Reporting Summary

Nature Research wishes to improve the reproducibility of the work that we publish. This form provides structure for consistency and transparency in reporting. For further information on Nature Research policies, see <u>Authors & Referees</u> and the <u>Editorial Policy Checklist</u>.

Statistical parameters

When statistical analyses are reported, confirm that the following items are present in the relevant location (e.g. figure legend, table legend, main text, or Methods section).

n/a	Confirmed	
☐	☒	The <u>exact sample size</u> (*n*) for each experimental group/condition, given as a discrete number and unit of measurement
☐	☒	An indication of whether measurements were taken from distinct samples or whether the same sample was measured repeatedly
☐	☒	The statistical test(s) used AND whether they are one- or two-sided *Only common tests should be described solely by name; describe more complex techniques in the Methods section.*
☐	☒	A description of all covariates tested
☐	☒	A description of any assumptions or corrections, such as tests of normality and adjustment for multiple comparisons
☐	☒	A full description of the statistics including <u>central tendency</u> (e.g. means) or other basic estimates (e.g. regression coefficient) AND <u>variation</u> (e.g. standard deviation) or associated <u>estimates of uncertainty</u> (e.g. confidence intervals)
☐	☒	For null hypothesis testing, the test statistic (e.g. *F*, *t*, *r*) with confidence intervals, effect sizes, degrees of freedom and *P* value noted *Give P values as exact values whenever suitable.*
☒	☐	For Bayesian analysis, information on the choice of priors and Markov chain Monte Carlo settings
☒	☐	For hierarchical and complex designs, identification of the appropriate level for tests and full reporting of outcomes
☐	☒	Estimates of effect sizes (e.g. Cohen's *d*, Pearson's *r*), indicating how they were calculated
☐	☒	Clearly defined error bars *State explicitly what error bars represent (e.g. SD, SE, CI)*

Our web collection on <u>statistics for biologists</u> may be useful.

Software and code

Policy information about <u>availability of computer code</u>

Data collection	WB: Image Lab （Version 4.0 build 16 Aug 1 2011） RT-PCR: Bio-Rad CFX Manager 3.1 （File Version：3.1.1517.0823） MRI: ParaVision 6.0.1 Gatan Microscopy Suite (Digital Micrograph, License ID: 750432155) GeneSnap (product version: 7.09; file version:7.09.17) SkanIt software 3.2 (Thermo scientific) Graphics software: Graphpad 5.0 Laser confocal microscope: ZEN 2012 x64 blue
Data analysis	Image analysis: Image-pro Plus 6.0; Colocalizer pro for mac 3.0.2 Data analysis: SPSS 16.0; EXCEL (Microsoft office 2016 Family and student edition) Image synthesis: Adobe Photoshop CS3 Extended 10.0 DTI: Diffusion_Toolkit_setup_v0.6.4.1; TrackVis_setup_v0.6.1; MRIcroN; Dcm2niigui1(April 2010)

For manuscripts utilizing custom algorithms or software that are central to the research but not yet described in published literature, software must be made available to editors/reviewers upon request. We strongly encourage code deposition in a community repository (e.g. GitHub). See the Nature Research <u>guidelines for submitting code & software</u> for further information.

Data

Policy information about <u>availability of data</u>

All manuscripts must include a <u>data availability statement</u>. This statement should provide the following information, where applicable:

- Accession codes, unique identifiers, or web links for publicly available datasets
- A list of figures that have associated raw data
- A description of any restrictions on data availability

All routine analysis methods are included in the Mthods section. The data that support the findings of this study are presented in the paper and supplementary materials and all raw data are available from the corresponding author upon reasonable request. The 5 published mRNA expression datasets (Glioblastoma-TCGA-540; Glioma-French-284, GSE16011; Glioblastoma-TCGA-395; Glioblastoma Stemcells-20, GSE15209; GSE67089) used in this study were obtained from R2, an Affymetrix analysis and visualization platform developed at the Department of Human Genetics at the Academic Medical Center-University of Amsterdam.

Field-specific reporting

Please select the best fit for your research. If you are not sure, read the appropriate sections before making your selection.

☒ Life sciences ☐ Behavioural & social sciences ☐ Ecological, evolutionary & environmental sciences

For a reference copy of the document with all sections, see nature.com/authors/policies/ReportingSummary-flat.pdf

Life sciences study design

All studies must disclose on these points even when the disclosure is negative.

Sample size	An estimated survival events would be needed to provide 70% power for a log-rank test, corresponding to survival rate of 0.4 vs. 0.1, with a two-sided α of 0.05.
Data exclusions	No data was excluded from the experiments.
Replication	At least 3 replicates were taken to verify the reproducibility of the experimental findings. All attempts at replication were successful.
Randomization	Animals from different cages in the same experimental group were selected to assure randomization. Animals and cultures were randomly assigned for the drug treatment and transduction with the different constructs.
Blinding	The investigators were blind to group allocation during data collection and analysis, including IHC, IF, and DTI.

Behavioural & social sciences study design

All studies must disclose on these points even when the disclosure is negative.

Study description	*Briefly describe the study type including whether data are quantitative, qualitative, or mixed-methods (e.g. qualitative cross-sectional, quantitative experimental, mixed-methods case study).*
Research sample	*State the research sample (e.g. Harvard university undergraduates, villagers in rural India) and provide relevant demographic information (e.g. age, sex) and indicate whether the sample is representative. Provide a rationale for the study sample chosen. For studies involving existing datasets, please describe the dataset and source.*
Sampling strategy	*Describe the sampling procedure (e.g. random, snowball, stratified, convenience). Describe the statistical methods that were used to predetermine sample size OR if no sample-size calculation was performed, describe how sample sizes were chosen and provide a rationale for why these sample sizes are sufficient. For qualitative data, please indicate whether data saturation was considered, and what criteria were used to decide that no further sampling was needed.*
Data collection	*Provide details about the data collection procedure, including the instruments or devices used to record the data (e.g. pen and paper, computer, eye tracker, video or audio equipment) whether anyone was present besides the participant(s) and the researcher, and whether the researcher was blind to experimental condition and/or the study hypothesis during data collection.*
Timing	*Indicate the start and stop dates of data collection. If there is a gap between collection periods, state the dates for each sample cohort.*
Data exclusions	*If no data were excluded from the analyses, state so OR if data were excluded, provide the exact number of exclusions and the rationale behind them, indicating whether exclusion criteria were pre-established.*
Non-participation	*State how many participants dropped out/declined participation and the reason(s) given OR provide response rate OR state that no participants dropped out/declined participation.*

Randomization	*If participants were not allocated into experimental groups, state so OR describe how participants were allocated to groups, and if allocation was not random, describe how covariates were controlled.*

Ecological, evolutionary & environmental sciences study design

All studies must disclose on these points even when the disclosure is negative.

Study description	*Briefly describe the study. For quantitative data include treatment factors and interactions, design structure (e.g. factorial, nested, hierarchical), nature and number of experimental units and replicates.*
Research sample	*Describe the research sample (e.g. a group of tagged Passer domesticus, all Stenocereus thurberi within Organ Pipe Cactus National Monument), and provide a rationale for the sample choice. When relevant, describe the organism taxa, source, sex, age range and any manipulations. State what population the sample is meant to represent when applicable. For studies involving existing datasets, describe the data and its source.*
Sampling strategy	*Note the sampling procedure. Describe the statistical methods that were used to predetermine sample size OR if no sample-size calculation was performed, describe how sample sizes were chosen and provide a rationale for why these sample sizes are sufficient.*
Data collection	*Describe the data collection procedure, including who recorded the data and how.*
Timing and spatial scale	*Indicate the start and stop dates of data collection, noting the frequency and periodicity of sampling and providing a rationale for these choices. If there is a gap between collection periods, state the dates for each sample cohort. Specify the spatial scale from which the data are taken*
Data exclusions	*If no data were excluded from the analyses, state so OR if data were excluded, describe the exclusions and the rationale behind them, indicating whether exclusion criteria were pre-established.*
Reproducibility	*Describe the measures taken to verify the reproducibility of experimental findings. For each experiment, note whether any attempts to repeat the experiment failed OR state that all attempts to repeat the experiment were successful.*
Randomization	*Describe how samples/organisms/participants were allocated into groups. If allocation was not random, describe how covariates were controlled. If this is not relevant to your study, explain why.*
Blinding	*Describe the extent of blinding used during data acquisition and analysis. If blinding was not possible, describe why OR explain why blinding was not relevant to your study.*

Did the study involve field work? ☐ Yes ☐ No

Field work, collection and transport

Field conditions	*Describe the study conditions for field work, providing relevant parameters (e.g. temperature, rainfall).*
Location	*State the location of the sampling or experiment, providing relevant parameters (e.g. latitude and longitude, elevation, water depth).*
Access and import/export	*Describe the efforts you have made to access habitats and to collect and import/export your samples in a responsible manner and in compliance with local, national and international laws, noting any permits that were obtained (give the name of the issuing authority, the date of issue, and any identifying information).*
Disturbance	*Describe any disturbance caused by the study and how it was minimized.*

Reporting for specific materials, systems and methods

Materials & experimental systems

n/a	Involved in the study
☐	☒ Unique biological materials
☐	☒ Antibodies
☐	☒ Eukaryotic cell lines
☒	☐ Palaeontology
☐	☒ Animals and other organisms
☐	☒ Human research participants

Methods

n/a	Involved in the study
☒	☐ ChIP-seq
☒	☐ Flow cytometry
☐	☒ MRI-based neuroimaging

Unique biological materials

Obtaining unique materials	All unique materials used in this study are readily available from the authors or from standard commercial sources.

Antibodies

Antibodies used	Notch1 (D1E11) XP® Rabbit mAb, Catalog#3608, Lot:5, CST, WB 1:1000, IF 1:100, IHC 1:200
	Sox2 (D6D9) XP® Rabbit mAb, Catalog#3579, Lot:8, CST, WB 1:1000, IF 1:100, IHC 1:200
	GAPDH (14C10) Rabbit mAb, Catalog#2118, Lot:10, CST, 1:1000
	Cleaved Notch1 9 (Val1744) (D3B8) Rabbit mAb, Catalog#4147, Lot:6, CST, 1:1000
	Jagged1 (Notch Receptor Interaction Antibody Sampler Kit), Catalog#8658, Lot:3, CST, 1:100
	Anti-Tau-1 Antibody, clone PC1C6, Alexa Fluor® 488 Conjugate, Catalog#MAB3420A4, Lot:2897241, merck, 1:100
	Anti-CD133 (PROM1) Antibody, Catalog#BM3141, Lot:3F10, BOSTER, Mouse, 1:100
	Anti-CD133 (PROM1) Antibody, Catalog #PB0168, BOSTER, Lot:ZP720BP20, Rabbit, 1:100
	Anti-MBP Antibody, Catalog#BA0094, Lot:10CM172, BOSTER, Rabbit, 1:100
	Anti-PBK Antibody, Catalog #PB0345, Lot:ZP1303BP03, BOSTER, Rabbit, 1:100
	Anti-CDC6 Antibody, Catalog#BA1726-1, Lot:12D24, BOSTER, Rabbit, 1:100
	Anti-CD44 antibody , Catalog#A00052, Lot:0001712Da455269, BOSTER, Rabbit, 1:100
	Anti-NF200 (NEFH) Antibody, Catalog#BM0100, Lot:N52, BOSTER, Mouse, 1:100
	Sox2 XP® Rabbit mAb (Alexa Fluor® 488 Conjugate), Catalog#5049, Lot:7, CST, Rabbit, 1:100
	Anti-activated Notch1, Catalog#ab8925, Lot:GR218543-56, abcam, Rabbit, 1:100
	Anti-SOX9 Antibody- ChIP Grade, Catalog#ab3697, Lot:GR38091-14, abcam, Rabbit, ChIP 1:100, WB 1:1000, IHC 1:200
	Anti-SOX9[EPR14335] (Alexa Fluor® 647), Catalog#ab196184, Lot:GR202358-2, abcam, Rabbit, 1:100, WB 1:1000
	SOX9 Monoclonal Antibody (1B11), Catalog#MA5-17177, LOT:PC183, THERMO, Mouse, EMSA 1:25, WB 1:1000
	Goat anti-Rabbit IgG (H+L) Cross-Adsorbed Secondary Antibody, Alexa Fluor 546, Catalog#A-11010, Lot:1809360, Invitrogen, 1:1000
	Goat anti-Mouse IgG (H+L) Cross-Adsorbed Secondary Antibody, Alexa Fluor 488, Catalog#A-11001, Lot:RJ242570, Invitrogen, 1:1000
	Goat anti-Rabbit IgG (H+L) Highly Cross-Adsorbed Secondary Antibody, Alexa Fluor Plus 647, Catalog#A32733, Lot:S1251745, Invitrogen, 1:1000
	Goat anti-Mouse IgG (H+L) Highly Cross-Adsorbed Secondary Antibody, Alexa Fluor 647, Catalog# A-21236, Lot:1887151, Invitrogen, 1:1000
	Goat IgG, whole molecule Catalog #BD0049, LOT:AA36131, Bioward, CHIP 1:100, EMSA 1:25
	PE Mouse Anti-Human CD133 Catalog#566593, 8171923, BD, 1:100
	Anti- RBP-Jκ, Catalog#sc-55019, Santa Cruz Biotechnology, mouse,1:100
	Anti-mouse IgG, HRP-linked Antibody, Catalog#7076, LOT: 33, CST, 1:3000
	Anti-rabbit IgG, HRP-linked Antibody, Catalog#7074, LOT: 25, CST, 1:3000
	Anti-SOX2 Antibody, Catalog#BM2014, LOT:10F10, BOSTER, Mouse, 1:100
Validation	Notch1 (D1E11) XP® Rabbit mAb, Catalog#3608, Lot:5, CST, WB1:1000, IF1:100, IHC 1:200
	https://www.cellsignal.com/products/primary-antibodies/notch1-d1e11-xp-rabbit-mab/3608?N=4294956287&Ntt=notch1&fromPage=plp
	Zhou, W., Tan, W., et al. Doxorubicin combined with Notch1-targeting siRNA for the treatm ent of gastric cancer.Oncol Lett. 2018 Sep;16(3):2805-2812
	Sox2 (D6D9) XP® Rabbit mAb, Catalog#3579, Lot:8, CST, 1:1000, IF1:100
	https://www.cellsignal.com/products/primary-antibodies/sox2-d6d9-xp-rabbit-mab/3579?N=4294956287&Ntt=sox2&fromPage=plp
	Ma, Y., Yu, T., et al.Preserving self-renewal of porcine pluripotent stem cells in serum-free 3i culture condition and independent of LIF and b-FGF cytokines. Cell Death Discov. 2018 Feb 14;4:21.
	GAPDH (14C10) Rabbit mAb, Catalog#2118, Lot:10, CST, 1:1000
	https://www.cellsignal.com/products/primary-antibodies/gapdh-14c10-rabbit-mab/2118?N=4294956287&Ntt=gapdh&fromPage=plp
	Matthes, F., Hettich, M. M., et al. Inhibition of the MID1 protein complex: a novel approach targeting APP protein synthesis. Cell Death Discov. 2018 Jan 29;4:4.
	Cleaved Notch1 9 (Val1744) (D3B8) Rabbit mAb, Catalog#4147, Lot:6, CST, 1:1000
	https://www.cellsignal.com/products/primary-antibodies/cleaved-notch1-val1744-d3b8-rabbit-mab/4147?N=4294956287&Ntt=nicd&fromPage=plp
	López-Arribillaga, E., Rodilla, V., et al. Manic Fringe deficiency imposes Jagged1 addiction to intestinal tumor cells. Nat Commun. 2018 Jul 31;9(1):2992.
	Jagged1 (Notch Receptor Interaction Antibody Sampler Kit), Catalog#8658, Lot:3, CST, 1:1000
	https://www.cellsignal.com/products/primary-antibodies/notch-receptor-interaction-antibody-sampler-kit/8658?N=4294956287&Ntt=jagged1&fromPage=plp
	Xie, W., Lu, J., et al. Matrine inhibits the proliferation and migration of lung cancer cells through regulation of the protein kinase B/glycogen synthase kinase-3β signaling pathways. Exp Ther Med. 2018 Aug;16(2):723-729.

Anti-Tau-1 Antibody, clone PC1C6, Alexa Fluor® 488 Conjugate, Catalog#MAB3420A4, Lot:2897241, merck, 1:100
http://www.merckmillipore.com/CN/zh/product/Anti-Tau-1-Antibody%2C-clone-PC1C6%2C-Alexa-Fluor-488-Conjugate,MM_NF-MAB3420A4

Anti-CD133 (PROM1) Antibody, Catalog#BM3141, Lot:3F10, BOSTER, Mouse, 1:100
http://www.boster.com.cn/product/anti-cd133-prom1-antibody_bm3141.html

Anti-CD133 (PROM1) Antibody, Catalog #PB0168, BOSTER, Lot:ZP720BP20, Rabbit, 1:100
http://www.boster.com.cn/product/anti-cd133-prom1-antibody_pb0168.html
Zhu T, Li X., et al. Reversion of malignant phenotypes of human glioblastoma cells by β-elemene through β-catenin-mediated regulation of stemness-, differentiation- and epithelial-to-mesenchymal transition-related molecules. J Transl Med. 2015 Nov 12;13:356.

Anti-MBP Antibody, Catalog#BA0094, Lot:10CM172, BOSTER, Rabbit, 1:100
http://www.boster.com.cn/product/anti-mbp-antibody_ba0094.html
Guangyi Zhao, Dan Li, et al. Nerve growth factor pretreatment inhibits lidocaine-induced myelin damage via increasing BDNF expression and inhibiting p38 mitogen activation in the rat spinal cord. Mol Med Rep. 2017 Oct; 16(4): 4678–4684.

Anti-PBK Antibody, Catalog #PB0345, Lot:ZP1303BP03, BOSTER, Rabbit, 1:100
http://www.boster.com.cn/product/anti-pbk-antibody_pb0345.html

Anti-CDC6 Antibody, Catalog#BA1726-1, Lot:12D24, BOSTER, Rabbit, 1:100
http://www.boster.com.cn/product/anti-cdc6-antibody_ba1726-1.html

Anti-CD44 antibody , Catalog#A00052, Lot:0001712Da455269, BOSTER, Rabbit, 1:100
http://www.boster.com.cn/product/anti-cd44-antibody_a00052.html
Wen X, Xie J, et al. The role of combining medroxyprogesterone 17-acetate with human menopausal gonadotropin in mouse ovarian follicular development. Sci Rep. 2018 Mar 13;8(1):4439.

Anti-NF200 (NEFH) Antibody, Catalog#BM0100, Lot:N52, BOSTER, Mouse, 1:100
http://www.boster.com.cn/product/anti-nf200-nefh-antibody_bm0100.html
Shao J, Cao J, et al. MicroRNA-30b regulates expression of the sodium channel Nav1.7 in nerve injury-induced neuropathic pain in the rat. Mol Pain. 2016 Oct 19;12.

Sox2 XP® Rabbit mAb (Alexa Fluor® 488 Conjugate), Catalog#5049, Lot:7, CST, Rabbit, 1:100
https://www.cst-c.com.cn/products/antibody-conjugates/sox2-d6d9-xp-rabbit-mab-alexa-fluor-488-conjugate/5049
Duan L, Wu XL, et al. Induction Effect to Apoptosis by Maitake Polysaccharide: Synergistic Effect of Its Combination With Vitamin C in Neuroglioma Cell. J Evid Based Complementary Altern Med. 2017 Oct;22(4):667-674.

Anti-activated Notch1, Catalog#ab8925, Lot:GR218543-56, abcam, Rabbit, 1:100
https://www.abcam.cn/activated-notch1-antibody-ab8925.html
Lu Y, Yan B, et al. Effect of midkine on gemcitabine resistance in biliary tract cancer. Int J Mol Med. 2018 Apr;41(4):2003-2011.

Anti-SOX9 Antibody- ChIP Grade, Catalog#ab3697, Lot:GR38091-14, abcam, Rabbit, ChIP 1:100, WB 1:1000, IHC 1:200
http://www.abcam.cn/sox9-antibody-chip-grade-ab3697.html
Ashraf S, Han IB, et al. Role of RHEB in Regulating Differentiation Fate of Mesenchymal Stem Cells for Cartilage and Bone Regeneration. Int J Mol Sci. 2017 Apr 24;18(4). pii: E880.

Anti-SOX9[EPR14335] (Alexa Fluor® 647), Catalog#ab196184, Lot:GR202358-2, abcam, Rabbit, 1:100
https://www.abcam.cn/sox9-antibody-epr14335-alexa-fluor-647-ab196184.html

SOX9 Monoclonal Antibody (1B11), Catalog#MA5-17177, LOT:PC183, THERMO, Mouse,EMSA 1:100, WB 1:1000
https://www.thermofisher.com/antibody/product/SOX9-Antibody-clone-1B11-Monoclonal/MA5-17177?pluginName=

Goat anti-Rabbit IgG (H+L) Cross-Adsorbed Secondary Antibody, Alexa Fluor 546, Catalog#A-11010, Lot:1809360, Invitrogen, 1:1000
https://www.thermofisher.com/antibody/product/Goat-anti-Rabbit-IgG-H-L-Cross-Adsorbed-Secondary-Antibody-Polyclonal/A-11010
Barca-Mayo O, Pons-Espinal M, et al. Astrocyte deletion of Bmal1 alters daily locomotor activity and cognitive functions via GABA signalling. Nat Commun. 2017 Feb 10;8:14336.

Goat anti-Mouse IgG (H+L) Cross-Adsorbed Secondary Antibody, Alexa Fluor 488, Catalog#A-11001, Lot:RJ242570, Invitrogen, 1:1000
https://www.thermofisher.com/antibody/product/Goat-anti-Mouse-IgG-H-L-Cross-Adsorbed-Secondary-Antibody-Polyclonal/A-11001?pluginName=
Caberlotto E, Ruiz L, et al. Effects of a skin-massaging device on the ex-vivo expression of human dermis proteins and in-vivo facial wrinkles. PLoS One. 2017 Mar 1;12(3):e0172624.

Goat anti-Rabbit IgG (H+L) Highly Cross-Adsorbed Secondary Antibody, Alexa Fluor Plus 647, Catalog#A32733, Lot:S1251745, Invitrogen, 1:1000
https://www.thermofisher.com/antibody/product/Goat-anti-Rabbit-IgG-H-L-Highly-Cross-Adsorbed-Secondary-Antibody-Polyclonal/A32733
Smith MD, Harley ME, et al. CCPG1 Is a Non-canonical Autophagy Cargo Receptor Essential for ER-Phagy and Pancreatic ER Proteostasis. Dev Cell. 2018 Jan 22;44(2):217-232.e11.

Goat anti-Mouse IgG (H+L) Highly Cross-Adsorbed Secondary Antibody, Alexa Fluor 647, Catalog# A-21236, Lot:1887151, Invitrogen, 1:1000
https://www.thermofisher.com/antibody/product/Goat-anti-Mouse-IgG-H-L-Highly-Cross-Adsorbed-Secondary-Antibody-Polyclonal/A-21236
Sohn J, Okamoto S, et al. Differential Inputs to the Perisomatic and Distal-Dendritic Compartments of VIP-Positive Neurons in Layer 2/3 of the Mouse Barrel Cortex. Front Neuroanat. 2016 Dec 20;10:124.

mouse monoclonal anti- RBP-Jκ (Santa Cruz Biotechnology, USA) Catalog # sc-55019
https://www.scbt.com/scbt/zh/product/rbp-jkappa-antibody-d-19?requestFrom=search
Zhang S, Kong S, et al. Uterine Rbpj is required for embryonic-uterine orientation and decidual remodeling via Notch pathway-independent and -dependent mechanisms. Cell Res. 2014 Aug;24(8):925-42.

rabbit monoclonal IgG1 anti-Sox2 Catalog #NB110-37235 NOVUS
https://www.novusbio.com/products/sox2-antibody_nb110-37235#PublicationSection
Luni C1,2, Giulitti S, et al. High-efficiency cellular reprogramming with microfluidics. Nat Methods. 2016 May;13(5):446-52.

PE Mouse Anti-Human CD133 Catalog#566593 BD
http://www.bdbiosciences.com/cn/applications/research/stem-cell-research/hematopoietic-stem-cell-markers/human/positive-markers/pe-mouse-anti-human-cd133-w6b3c1-also-known-as-w6b3/p/566593
Koerner SP, André MC, et al. An Fc-optimized CD133 antibody for induction of NK cell reactivity against myeloid leukemia.. Leukemia. 2017; 31(2):459-469.

Goat IgG, whole molecule Catalog #BD0049 Bioward
https://www.bioworlde.com/Goat-IgG,whole-molecule(BD0049).html
Kuang JY, Guo YF, et al. Connexin 43 C-terminus directly inhibits the hyperphosphorylation of Akt/ERK through protein-protein interactions in glioblastoma. Cancer Sci. 2018 Aug;109(8):2611-2622.

Anti-mouse IgG, HRP-linked Antibody, Catalog #7076, CST
https://www.cellsignal.com/products/secondary-antibodies/anti-mouse-igg-hrp-linked-antibody/7076?site-search-type=Products&N=4294956287&Ntt=7076s&fromPage=plp&_requestid=340768
Song K, Yuan Y, et al. ERBB3, IGF1R, and TGFBR2 expression correlate with PDGFR expression in glioblastoma and participate in PDGFR inhibitor resistance of glioblastoma cells. Am J Cancer Res. 2018 May 1;8(5):792-809.

Anti-rabbit IgG, HRP-linked Antibody, Catalog#7074, CST
https://www.cellsignal.com/products/secondary-antibodies/anti-rabbit-igg-hrp-linked-antibody/7074
Song K, Yuan Y, et al. ERBB3, IGF1R, and TGFBR2 expression correlate with PDGFR expression in glioblastoma and participate in PDGFR inhibitor resistance of glioblastoma cells. Am J Cancer Res. 2018 May 1;8(5):792-809.

Anti-SOX2 Antibody, Catalog#BM2014, LOT:10F10, BOSTER, Mouse, 1:100
http://www.boster.com.cn/product/anti-sox2-antibody_bm2014.html

Eukaryotic cell lines

Policy information about cell lines

Cell line source(s)	The human glioma cell line U87 and the mouse glioma cell line were purchased from American Type Culture Collection (ATCC, USA). Three human glioma samples (GBM1-3) were successfully used for a primary culture.
Authentication	All cell lines used in this study were identified by STR DNA typing.
Mycoplasma contamination	All cell lines tested negative for mycoplasma contamination.
Commonly misidentified lines (See ICLAC register)	No cell line used in this paper are listed in the database of commonly misidentified cell lines maintained by ICLAC.

Palaeontology

Specimen provenance	*Provide provenance information for specimens and describe permits that were obtained for the work (including the name of the issuing authority, the date of issue, and any identifying information).*
Specimen deposition	*Indicate where the specimens have been deposited to permit free access by other researchers.*
Dating methods	*If new dates are provided, describe how they were obtained (e.g. collection, storage, sample pretreatment and measurement), where they were obtained (i.e. lab name), the calibration program and the protocol for quality assurance OR state that no new dates are provided.*

☐ Tick this box to confirm that the raw and calibrated dates are available in the paper or in Supplementary Information.

Animals and other organisms

Policy information about studies involving animals; ARRIVE guidelines recommended for reporting animal research

Laboratory animals	NOD/SCID mice, 4-week-old; Thy1-EGFP transgenic mice.
Wild animals	The study did not involve wild animals.
Field-collected samples	The study did not involve samples from the field.

Human research participants

Policy information about studies involving human research participants

Population characteristics	Two hundred and eighteen human research participants (Paraffin-embedded samples) in total: aged from 4 to 71; 85 female and 133 male; 106 Astrocytoma, 27 Oligodendroglioma, 16 Astrocytoma-Oligodendroglioma, 1 Ependymocytoma-Astrocytoma, 1 ganglioneuroma-Astrocytoma, 67 GBM; 31 Surgery, 30 Surgery+chemotherapy, 62 Surgery+radiotherapy, 95 Surgery+chemotherapy+radiotherapy.
Recruitment	Retrospective study. Paraffin-embedded samples from glioma patients were obtained during surgery at the Southwest Hospital and TianTan Hospital (218 cases between 2005 and 2009; among them, 108 cases had follow-up data).

ChIP-seq

Data deposition

☐ Confirm that both raw and final processed data have been deposited in a public database such as GEO.

☐ Confirm that you have deposited or provided access to graph files (e.g. BED files) for the called peaks.

Data access links *May remain private before publication.*	*For "Initial submission" or "Revised version" documents, provide reviewer access links. For your "Final submission" document, provide a link to the deposited data.*
Files in database submission	*Provide a list of all files available in the database submission.*
Genome browser session (e.g. UCSC)	*Provide a link to an anonymized genome browser session for "Initial submission" and "Revised version" documents only, to enable peer review. Write "no longer applicable" for "Final submission" documents.*

Methodology

Replicates	*Describe the experimental replicates, specifying number, type and replicate agreement.*
Sequencing depth	*Describe the sequencing depth for each experiment, providing the total number of reads, uniquely mapped reads, length of reads and whether they were paired- or single-end.*
Antibodies	*Describe the antibodies used for the ChIP-seq experiments; as applicable, provide supplier name, catalog number, clone name, and lot number.*
Peak calling parameters	*Specify the command line program and parameters used for read mapping and peak calling, including the ChIP, control and index files used.*
Data quality	*Describe the methods used to ensure data quality in full detail, including how many peaks are at FDR 5% and above 5-fold enrichment.*
Software	*Describe the software used to collect and analyze the ChIP-seq data. For custom code that has been deposited into a community repository, provide accession details.*

Flow Cytometry

Plots

Confirm that:

☐ The axis labels state the marker and fluorochrome used (e.g. CD4-FITC).

☐ The axis scales are clearly visible. Include numbers along axes only for bottom left plot of group (a 'group' is an analysis of identical markers).

☐ All plots are contour plots with outliers or pseudocolor plots.

☐ A numerical value for number of cells or percentage (with statistics) is provided.

Methodology

Sample preparation	*Describe the sample preparation, detailing the biological source of the cells and any tissue processing steps used.*
Instrument	*Identify the instrument used for data collection, specifying make and model number.*
Software	*Describe the software used to collect and analyze the flow cytometry data. For custom code that has been deposited into a community repository, provide accession details.*
Cell population abundance	*Describe the abundance of the relevant cell populations within post-sort fractions, providing details on the purity of the samples and how it was determined.*
Gating strategy	*Describe the gating strategy used for all relevant experiments, specifying the preliminary FSC/SSC gates of the starting cell population, indicating where boundaries between "positive" and "negative" staining cell populations are defined.*

☐ Tick this box to confirm that a figure exemplifying the gating strategy is provided in the Supplementary Information.

Magnetic resonance imaging

Experimental design

Design type	To trace the nerve fibers distant to tumor
Design specifications	At least three mice per group
Behavioral performance measures	No behavioral performance was measuredt

Acquisition

Imaging type(s)	Diffusion tensor imaging (DTI) and fiber tracking
Field strength	7.0 Tesla
Sequence & imaging parameters	4-shot spin-echo echo planar imaging sequence,TR/TE3000 ms/26 ms, FOV 25 mm×25 mm, slice thickness 0.5 mm, interslice gap: 0.5 mm, matrix size 128×128
Area of acquisition	*State whether a whole brain scan was used OR define the area of acquisition, describing how the region was determined.*

Diffusion MRI   ☒ Used   ☐ Not used

Preprocessing

Preprocessing software	DTI preprocessing was performed using the Functional Magnetic Resonance Imaging of the Brain Software Library (FSL4.1: http://www.fmrib.ox.ac.uk/fsl). The DTI data were corrected for head movement and eddy current distortions with the non-diffusion-weighted image (the b0 image) as a reference image.
Normalization	N/A
Normalization template	N/A
Noise and artifact removal	N/A
Volume censoring	To minimize motion artefacts, the mouse was secured in the animal holder in a supine position with the head secured in a nose cone (PMID:27467829).

Statistical modeling & inference

Model type and settings	N/A
Effect(s) tested	N/A

Specify type of analysis: ☒ Whole brain   ☐ ROI-based   ☐ Both

Statistic type for inference (See Eklund et al. 2016)	N/A
Correction	N/A

Models & analysis

n/a	Involved in the study
☒	☐ Functional and/or effective connectivity
☒	☐ Graph analysis
☒	☐ Multivariate modeling or predictive analysis

Functional and/or effective connectivity

> *Report the measures of dependence used and the model details (e.g. Pearson correlation, partial correlation, mutual information).*

Graph analysis

> *Report the dependent variable and connectivity measure, specifying weighted graph or binarized graph, subject- or group-level, and the global and/or node summaries used (e.g. clustering coefficient, efficiency, etc.).*

Multivariate modeling and predictive analysis

> *Specify independent variables, features extraction and dimension reduction, model, training and evaluation metrics.*